DALTON
FULL PAPER

First high-nuclearity thallium–palladium carbonyl phosphine cluster, $[Tl_2Pd_{12}(CO)_9(PEt_3)_9]^{2+}$, and its initial mistaken identity as the unknown Au_2Pd_{12} analogue: structure-to-synthesis approach concerning its formation †

Sergei A. Ivanov, Rita V. Nichiporuk, Eugeny G. Mednikov and Lawrence F. Dahl

Department of Chemistry, University of Wisconsin-Madison, Madison, WI 53706, USA

Received 2nd May 2002, Accepted 22nd August 2002
First published as an Advance Article on the web 18th October 2002

Our exploratory research objective to obtain new high-nuclearity Au–Pd carbonyl phosphine clusters from reactions in DMF of preformed $Pd_{10}(CO)_{12}(PEt_3)_6$ with $Au(PPh_3)Cl$ in the presence of $TlPF_6$ (a frequently utilized chloride-scavenger) has given rise unexpectedly in 40% yield to the first example of a heterometallic Tl–Pd carbonyl phosphine cluster, $[Tl_2Pd_{12}(CO)_9(PEt_3)_9]^{2+}$ (**1-Et**), as the $[PF_6]^-$ salt. Its initial incorrect formulation as the unknown Au_2Pd_{12} cluster, obtained from a well-refined low-temperature CCD X-ray diffraction analysis of its crystal structure, was primarily based upon its related molecular geometry to that of the previously reported $[Au_2Pd_{14}(CO)_9(PMe_3)_{11}]^{2+}$ (as the $[PF_6]^-$ salt) prepared from an analogous reaction of $Pd_8(CO)_8(PMe_3)_7$ and $Au(PCy_3)Cl$ in the presence of $TlPF_6$. (Because X-ray scattering occurs *via* the electrons of atoms, an assignment in the crystal-structure determination of **1-Et** of the two independent "heavy" atoms as either Tl (at. no. 81) or Au (at. no. 79) would result in non-distinguishable refinements). **1-Et** was originally characterized by IR and $^{31}P\{^1H\}$ NMR; attempted MALDI-ToF mass-spectrometric measurements were unsuccessful. The geometrically unprecedented *pseudo*-C_{3h} core of **1-Et** may *now* be described as edge-fusions of three trigonal bipyramidal Pd_5 fragments to a central trigonal bipyramidal Tl_2Pd_3 kernel. Its formation was *originally* viewed as the condensation product of three partially ligated butterfly $Pd_4(CO)_3(PEt_3)_3$ fragments that are also linked to and stabilized by two capping naked Au^+ cations. This proposed "structure-to-synthesis" approach led to the isolation of **1-Et** in *ca.* 90% yield from the reaction in DMF of the butterfly $Pd_4(CO)_5(PEt_3)_4$ with the phosphine-scavenger $Au(SMe_2)Cl$ together with $TlPF_6$. Our later realization and resulting conclusive evidence that its metal-core stoichiometry is Tl_2Pd_{12} instead of Au_2Pd_{12} was a consequence of: (1) our bothersome inability based upon a presumed Au_2Pd_{12} core-geometry to interpret its complex $^{31}P\{^1H\}$ NMR spectrum despite $^{31}P\{^1H\}$ COSY experiments clearly showing couplings between the seven major resonances that are consistent with *intramolecular* processes involving only *one* species; (2) our subsequent direct preparation of the same Tl_2Pd_{12} cluster (90% yield) from the reaction in THF of $Pd_4(CO)_5(PEt_3)_4$ with $TlPF_6$ (mol. ratio, 3/2), and the ensuing low-temperature CCD X-ray determination revealing a virtually identical solid-state structure (as expected) but with $^{31}P\{^1H\}$ NMR measurements displaying an analogous complex spectrum that now can be interpreted; and (3) an elemental analysis (Tl, Au, Pd, P), which had been delayed because of the misleading confidence concerning our initially assigned stoichiometry, that ascertained its present formulation; noteworthy is that an elemental analysis of a sample of this compound would *not* disclose its true identity unless directly tested for Tl (and the absence of Au). Gradient-corrected DFT calculations performed on the PH_3-model of the crystallographically known butterfly $Pd_4(CO)_5(PPh_3)_4$ and on its hypothetical Tl^+, Au^+, and $[Au(PH_3)]^+$ adducts (where the optimized geometries consisted of a trigonal bipyramidal MPd_4 core with an equatorial $M = Tl^+$, Au^+, or $[Au(PH_3)]^+$) revealed: (a) that the monocationic Tl^+ charge is primarily localized on thallium in contrast to the monocationic Au^+ charge being much more delocalized over the entire molecule with charge density having been withdrawn mainly from CO ligands (relative to that of the neutral $Pd_4(CO)_5(PH_3)_4$); (b) that the interactions of Tl^+, Au^+, or $[Au(PH_3)]^+$ adducts with a stable butterfly $Pd_4(CO)_5(PH_3)_4$ model are energetically favorable processes, with Au^+ bonding being stronger than Tl^+ bonding to $Pd_4(CO)_5(PH_3)_4$; and (c) that the presence of an additional PH_3 ligand on the Au^+ significantly weakens the Au–Pd bonding interactions such that its bonding energy is comparable with that of the Tl–Pd interactions.

Introduction

Considerable interest in bimetallic Au–Pd and Au–Pt clusters stems from their potential to serve as models for particles found in supported gold alloy catalysts.[1] Significant increases in activity and selectivity were reported upon the incorporation of gold into catalytically active transition metal clusters. Pignolet and coworkers[2] observed from extensive studies that gold clusters possessing electron-rich Pd and Pt metals have the greatest potential for catalytic activity, given the prominence of these metals in commercial catalysts. They found that phosphine-stabilized Au–Pd and Au–Pt clusters are very active homogeneous catalysts for the H_2–D_2 equilibration reaction and $D_2(g)$–$H_2O(l)$ isotope exchange in solution.[2c–g] In addition, they showed that the same Au–Pt clusters deposited on silica and alumina supports have similar reactivities.[2h] Bimetallic Au–Pd carbonyl clusters would be of particular utility as ideal

† Dedicated to Mike Mingos in honor of his many exceptional theoretical/experimental contributions to metal cluster research during his illustrious academic career in Inorganic/Organometallic Chemistry at Oxford University and Imperial College of Science, Technology, and Medicine.

 DOI: 10.1039/b204276m

precursors in generating decarbonylated support-attached species that may function in an analogous fashion to that of homogeneous and heterogeneous catalysts.[3] For example, the SiO_2-supported $[Pd_6Fe_6H(CO)_{24}]^{3-}$ trianion was used to obtain a Pd–Fe bimetallic catalyst that exhibited high selectivity toward methanol syntheses from CO/H_2 reaction.[4] Another intriguing future aspect of special relevance to nanoscience research is whether decarbonylated support-attached homometallic/heterometallic cores of any of these clusters can be appropriately utilized as nanostructured "building blocks" in the construction of complex assemblies.

Since there are relatively few well-characterized high-nuclearity Group 10/Group 11 bimetallic carbonyl species, a major part of our recent research has focused upon the synthesis and characterization of nanosized Pd/(coinage metal) carbonyl clusters. The most commonly employed method to prepare Au–Pd clusters is by direct combination of monometallic palladium precursors of both Pd(II) and Pd(0) types of compounds (*e.g.*, $Pd(OAc)_2$ or $Pd(PPh_3)_4$) with Au(I) complexes (*e.g.*, $Au(PPh_3)NO_3$) in the presence of a reducing agent ($NaBH_4$ or H_2).[5] The major role of the reducing agent is to reduce gold(I) to a non-integral oxidation state, which leads to the condensation of quasi-gold metal atoms into a cluster with incorporation of the Group 10 transition metals. This method usually gives rise to small bimetallic clusters[2a] but also has resulted in the isolation of non-crystalline bimetallic nanocolloidal particles.[5] However, notable exceptions were reactions of the monometallic $Pd(PEt_3)_2Cl_2$ and $Au(PPh)_3Cl$ in DMF with NaOH under CO atmosphere, which resulted in the truly remarkable homopalladium $Pd_{145}(CO)_x(PEt_3)_{30}$ and as by-products two large neutral Au–Pd clusters, $Au_2Pd_{21}(CO)_{20}(PEt_3)_{10}$ and $Au_2Pd_{41}(CO)_{27}(PEt_3)_{15}$.[6]

A relatively unexplored way to synthesize Au–Pd carbonyl clusters would involve reactions of small palladium carbonyl phosphine clusters with different gold(I) compounds. There is only one reported example where this synthetic pathway was utilized to prepare a high-nuclearity Au–Pd cluster. Mingos *et al.*[7] showed that $Pd_8(CO)_8(PMe_3)_7$[8] can be effectively used as a Pd precursor, as demonstrated by its reaction in THF with $Au(PCy_3)Cl$ in the presence of excess $TlPF_6$ that resulted in the $[Au_2Pd_{14}(\mu_3\text{-}CO)_7(\mu_2\text{-}CO)_2(PMe_3)_{11}]^{2+}$ dication, **2-Me**, as the $[PF_6]^-$ salt (*vide infra*). The fact that this synthetic approach afforded **2-Me**, which has a highly unusual Au_2Pd_{14} core-geometry, suggested that this preparative pathway should be extensively investigated.

Comprehensive reviews by Burrows and Mingos[9] on palladium cluster compounds and Group 10 metal *triangulo* clusters are especially informative in revealing the availability of a considerable number of small palladium clusters as possible precursors.We selected another palladium carbonyl cluster, $Pd_{10}(CO)_{12}(PEt_3)_6$ (**3-Et**), for reactions with $Au(PPh_3)Cl$. This Pd_{10} cluster was first synthesized by Mednikov *et al.*[10a] but more recently was prepared by a different method and characterized by Mingos and Hill[10b] from crystallographic/spectroscopic studies. Our choice was dictated by several reasons: (1) **3-Et** is known to be reactive under an inert atmosphere (*i.e.*, it is stable only under CO);[10a] (2) Mednikov *et al.*[11] showed **3-Et** to be an excellent precursor for the synthesis of larger homopalladium clusters including $Pd_{16}(CO)_{13}(PEt_3)_9$,[11a] $Pd_{23}(CO)_{22}(PEt_3)_{10}$,[11b] $Pd_{23}(CO)_{20}(PEt_3)_8$,[11c] $Pd_{34}(CO)_{24}(PEt_3)_{12}$,[11d] and $Pd_{38}(CO)_{28}(PEt_3)_{12}$;[11d,e] (3) in solution **3-Et** undergoes reversible conversion into $Pd_4(CO)_5(PEt_3)_4$, which can be viewed as a structural building block in the formation of the Pd_8, Pd_{10}, Pd_{16}, and Pd_{23} clusters; (4) its synthetic procedure is well-established, and this precursor can be obtained in high yield (~90%) from commercially available materials – namely, $Pd(OAc)_2$, PEt_3, and CO.[10a,11]

Herein we report: (1) our initial reactions in DMF of $Pd_{10}(CO)_{12}(PEt_3)_6$ (**3-Et**) with $Au(PPh_3)Cl$ in the presence of $TlPF_6$ that gave rise to the isolation of **1-Et** in 40% yield; and (2) its crystal-structure analysis that resulted in an incorrect atom-labeling assignment of the $[Au_2Pd_{12}(CO)_9(PEt_3)_9]^{2+}$ dication instead of the crystallographically indistinguishable $[Tl_2Pd_{12}(CO)_9(PEt_3)_9]^{2+}$ dication. We demonstrate a general structure-to-synthesis approach in metal cluster chemistry: namely, a particular geometry (originally presumed in this case to have a Au_2Pd_{12} core) suggesting an alternative preparative pathway, from which **1-Et** was synthesized in a higher yield (*ca.* 90%) from reactions in DMF of $Pd_4(CO)_5(PEt_3)_4$ with the phosphine-scavenger $Au(SMe_2)Cl$) in the presence of $TlPF_6$. We then present the tortuous trail of combined factual observations, $^{31}P\{^1H\}$ NMR inconsistency, and special circumstances, including its direct preparation (90% yield) from $Pd_4(CO)_5(PEt_3)_4$ with $TlPF_6$ (mole ratio, 3/2) in THF that led to the ultimate correct identity of **1-Et** (*i.e.*, ascertained from an elemental analysis). In addition to the spectroscopic IR and $^{31}P\{^1H\}$ NMR characterization that is consistent with the solid-state geometry of **1-Et**, we also provide herein the results of gradient-corrected DFT calculations on the PH_3-substituted model of the crystallographically known butterfly $Pd_4(CO)_5(PPh_3)_4$ molecule and on its hypothetical Tl^+, Au^+, or $[Au(PH_3)]^+$ adducts in order to determine the resulting geometrical/electronic consequences.

Results and discussion

Structural features of $[Tl_2Pd_{12}(CO)_9(PEt_3)_9]^{2+}$ (1-Et)

The structural determination and refinement of the original CCD X-ray data set of **1-Et** were based upon the initial assignment of the metal core as Au_2Pd_{12}. A subsequent CCD X-ray data set was collected from a crystal of a sample isolated from the direct reaction of $Pd_{10}(CO)_{12}(PEt_3)_6$ (**1-Et**) with $TlPF_6$ (without Au(I) reagent). As expected, the resulting molecular parameters obtained from complete refinement of both data sets are virtually identical; the molecular parameters presented herein are from the first data set.

The $[PF_6]^-$ salt of **1-Et** crystallizes in the orthorhombic *Pbca* space group; the unit cell contains eight cations (**1-Et**) and sixteen $[PF_6]^-$ anions with one cation and two anions comprising the crystallographically independent unit. No solvated molecules were found in the crystal structure.

Fig. 1 gives the geometry of the Tl_2Pd_{12} core in **1-Et**, while Fig. 2 presents the molecular geometry of **1-Et** (without the P-attached ethyl substituents). Fig. 1 also shows that the geometrically unprecedented Tl_2Pd_{12} core of **1-Et** may be viewed as three trigonal bipyramidal Pd_5 fragments that each share two vertices (or one edge) with a centered trigonal bipyramidal Tl_2Pd_3 fragment.

This Tl_2Pd_{12} core ideally conforms to C_{3h} symmetry with the principal threefold axis passing through the two thallium atoms; the horizontal mirror plane contains the central triangle of three palladium atoms (*viz.*, Pd(4), Pd(5), Pd(12)) and the three outer axial palladium atoms (*viz.*, Pd(1), Pd(8), Pd(11)) of the three threefold-related Pd_5 trigonal bipyramids. The average perpendicular displacement of these six Pd atoms from the mean σ_h plane is 0.04 Å. Nevertheless, a significant difference is found betweeen the mean of 2.94 Å for the six Tl(1)–Pd distances (range, 2.858(1)–3.042(1) Å) and that of 2.87 Å for the six Tl(2)–Pd distances (range, 2.847(1)–2.930(1) Å); this large variation points to a breakdown of the σ_h mirror-plane symmetrty and suggests the non-equivalence of the two Tl atoms in the crystalline state (in accordance with one F atom of a $[PF_6]^-$ anion being directed toward Tl(1) at an ion-pair distance of 3.183 Å.

Each of the mirror-related six-coordinate non-ligated Tl atoms is connected to the central Pd_3 triangle and to one of the mirror-related equatorial Pd atoms of the edge-fused Pd_5 trigonal bipyramids. Each of the three palladium atoms (*viz.*, Pd(4), Pd(5), Pd(12)) of the central Pd_3 triangle corresponds to

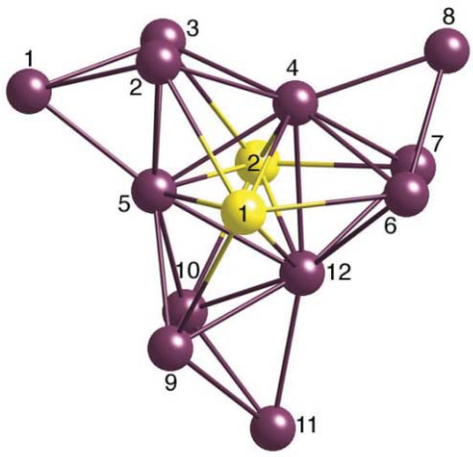

Fig. 1 Tl_2Pd_{12} core-architecture in $[Tl_2Pd_{12}(CO)_9(PEt_3)_9]^{2+}$ dication, **1-Et** ($[PF_6]^-$ salt). This core approximately conforms to C_{3h} (3/*m*) symmetry with the principal 3-fold axis passing through Tl(1) and Tl(2) and with the horizontal σ_h mirror passing through the central triangular Pd(4), Pd(5), and Pd(12) and through Pd(1), Pd(8), and Pd(11). Its overall geometry may be viewed as edge-fusions of three Pd_5-trigonal bipyramids to a central Tl_2Pd_3 trigonal bipyramid. Its chemical formulation may be described as a condensation product of three partially ligated butterfly $Pd_4(CO)_3(PEt_3)_3$ fragments that are stabilized by two capping naked Tl^+ cations.

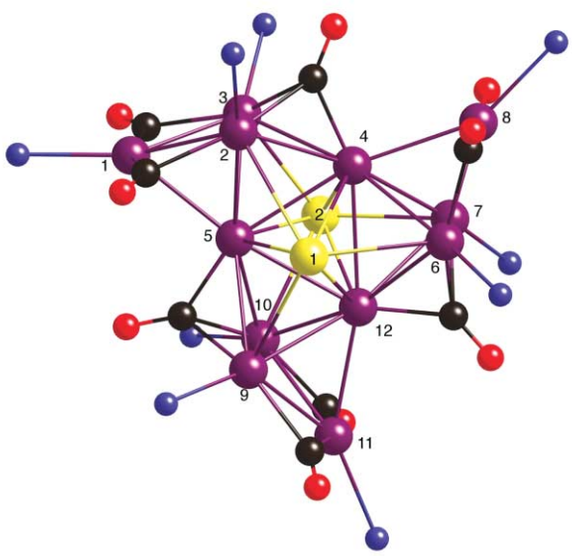

Fig. 2 Molecular structure of $[Tl_2Pd_{12}(\mu_2\text{-}CO)_6(\mu_3\text{-}CO)_3(PEt_3)_9]^{2+}$ dication (**1-Et**) with P-attached Et substituents omitted for clarity. Its overall configuration ideally maintains C_{3h} symmetry with the σ_h mirror passing through the central triangular Pd(4), Pd(5), and Pd(12) and through the outer Pd(1), Pd(8), and Pd(11) and their coordinated P atoms, and the three triply bridging COs. The two Tl atoms each cap the three Pd atoms of the central triangle and one of the two equatorial Pd atoms of each Pd_5 trigonal bipyramid. The three central triangular Pd atoms, that do not possess phosphine ligands, have the highest coordination numbers with each being connected to both Tl and eight Pd atoms and to one triply bridging CO. Each of the 3-fold related outer Pd(1), Pd(8), and Pd(11) has an approximately localized trigonal-planar ligand arrangement comprised of its attached P atom and two doubly bridging COs.

an axial atom of the Pd_5 trigonal bipyramid and an equatorial atom of an adjacent Pd_5 trigonal bipyramid. The two thallium atoms function as capping atoms that additionally link the three trigonal bipyramids and thereby stabilize **1-Et**. Metal-coordination numbers of the three different palladium atoms under assumed C_{3h} symmetry are only three for Pd(1) and its other two equivalent axial atoms, five for Pd(2) and its other five equivalent equatorial atoms, and nine for Pd(4) and its other two equivalent central-triangular atoms (Fig. 1). Upon ligation, the number of atom-connectivities increases to six for Pd(1), to eight for Pd(2), and to ten for Pd(4). Mean Tl–Pd and Pd–Pd distances under assumed C_{3h} symmetry are presented in Table 1.

Table 1 Important mean structural parameters for Tl_2Pd_{12} core of $[Tl_2Pd_{12}(CO)_9(PEt_3)_9]^{2+}$ (**1-Et**)

Connectivity[a]	*N*[b]	Mean/Å	Range[e]/Å
Pd(A)–Pd(B)	6	2.73	2.711–2.748
Pd(A)–Pd(C)	3	2.745	2.731–2.764
Pd(C)–Pd(B)[c]	6	2.77	2.751–2.795
Pd(C)–Pd(B)[d]	6	2.83	2.800–2.862
Pd(C)–Pd(C′)	3	2.90	2.858–2.945
Pd(B)–Pd(B′)	3	2.83	2.811–2.848
Tl–Pd(C)	6	2.89	2.847–2.930
Tl–Pd(B)	6	2.92	2.843–3.042
Tl(1) ⋯ Tl(2)	1	4.705	—

[a] Designations (based upon Fig. 2) of equivalent Pd atoms under *pseudo*-C_{3h} symmetry are as follows: Pd(A) denotes Pd(1), Pd(8), Pd(11); Pd(B) denotes Pd(2), Pd(3), Pd(6), Pd(7), Pd(9), Pd(10); Pd(C) denotes Pd(4), Pd(5), Pd(12). [b] *N* designates multiplicity of individual connectivities under *pseudo*-C_{3h} symmetry. [c] Bridged with Pd(A). [d] Unbridged. [e] Estimated uncertainties of individual Tl–Pd and Pd–Pd distances are 0.001 Å.

Inclusion of the nine Pd-attached triethylphosphine P atoms and nine bridging COs (shown in Fig. 2) ideally maintains the *pseudo*-C_{3h} symmetry of **1-Et**. Six of the nine carbonyl ligands edge-bridge two Pd atoms, while the remaining three carbonyl ligands cap three Pd atoms.

Spectroscopic characterization of $[Tl_2Pd_{12}(CO)_9(PEt_3)_9]^{2+}$ (1-Et)

A solid-state infrared spectrum of crystals of **1-Et** in Nujol revealed two strong carbonyl stretching frequencies at 1863 and 1836 cm^{-1} along with a broad band centered at *ca.* 1800 cm^{-1}. This spectrum is consistent with the *pseudo*-C_{3h} symmetry of **1**, for which three absorption bands of E′, A″, and E′ symmetry would be expected (*i.e.*, with the first two bands associated with μ_2-CO and the last one with μ_3-CO vibrations). Analogous IR bands were observed in an IR spectrum of **1-Et** in THF (1870, 1843, and 1805 cm^{-1}).

A $^{31}P\{^1H\}$ NMR spectrum of **1-Et** in THF-d_8 at room temperature (Fig. 5a) consists of 10 broad singlets (*i.e.*, half-width at half-height for most intense peaks is *ca.* 0.05 ppm) at δ_A 30.2, δ_B 28.7, δ_C 28.4, δ_D 26.2, δ_H 25.4, δ_I 24.6, δ_J 23.8, δ_E 22.2, δ_F 21.5, and δ_G 21.2 ppm with relative intensities 1 : 1 : 2 : 2 : 0.8 : 0.8 : 0.4 : 1 : 2 : 1, respectively, plus a septet resonance (due to $[PF_6]^-$) centered at −140 ppm; a low-temperature NMR spectrum (190 K) did not clarify the picture. Except for a slight temperature induced downfield shift ($\Delta \sim 1.0$ ppm) of all signals, no indication of coalescence or resolution was observed. Room-temperature $^{31}P\{^1H\}$ NMR spectra of **1-Et** in acetone-d_6 and THF-d_8 were analogous except for a ~2 ppm downfield shift of all signals in THF-d_8 solution compared to those in acetone-d_6. The similarity of the $^{31}P\{^1H\}$ NMR spectra of **1-Et** to variations in temperature and solvent indicated that all observed signals are characteristic of **1-Et**.

On the basis of the presumed Au_2Pd_{12} core-geometry, efforts to interpret the complex $^{31}P\{^1H\}$ NMR spectrum were unsuccessful (at that time we had not performed the $^{31}P\{^1H\}$ COSY NMR experiment).[12] Mingos *et al.*[7] also encountered a similar problem in their attempt to interpret an eight-(broad line) $^{31}P\{^1H\}$ NMR ($CDCl_3$) solution spectrum at room and low temperatures of $[Au_2Pd_{14}(CO)_9(PMe_3)_{11}]^{2+}$ (**2-Me**). They proposed that the cluster is highly fluxional in solution and undergoes a series of rearrangements with low kinetic barriers. Consequently, we likewise assumed that the presumed Au_2Pd_{12} framework in **1-Et** is stereochemically nonrigid in solution on the NMR timescale.

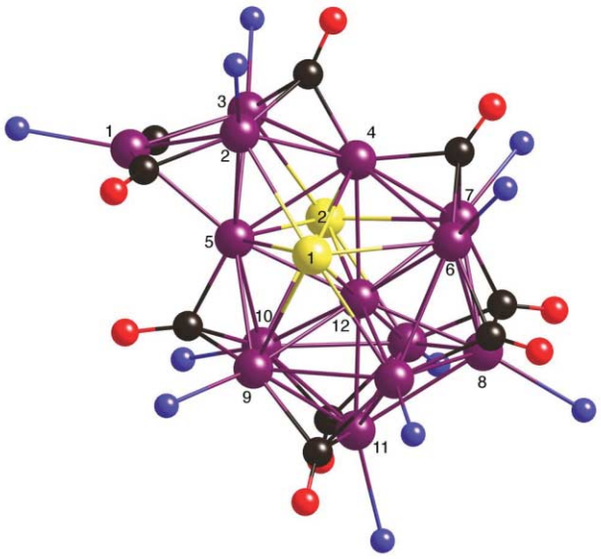

Fig. 3 Molecular structure of $[Au_2Pd_{14}(\mu_2\text{-}CO)_2(\mu_3\text{-}CO)_7(PMe_3)_{11}]^{2+}$ (**2-Me**) with P-attached Me substituents omitted for clarity. This dication (as the $[PF_6]^-$ salt) was prepared and characterized by Mingos *et al.*[7] The metal framework (renumbered to coincide with that of **1-Et**) is best described as a Pd-centered Au_2Pd_{11} icosahedron that shares a common edge, Pd(4)–Pd(5), with a Pd_5 trigonal bipyramid. A crystallographic mirror plane passes through the icosahedral-centered Pd(12), through the edge-sharing Pd(4) and Pd(5), through Pd(1), Pd(8), Pd(11) and their attached P atoms, and through five of the seven triply bridging COs. A highly unusual structural feature is that each of the two mirror-related surface icosahedral Au atoms does not possess a phosphine ligand but instead is connected with seven Pd atoms. The only two Pd atoms that likewise are not coordinated to a phosphine ligand are Pd(4) and Pd(5) that edge-fuse the icosahedron and trigonal bipyramid. Except for the icosahedral-centered Pd(12), both of these Pd atoms have the highest coordination numbers: namely, to nine metal atoms and one triply bridging CO for Pd(5) and to eight metal atoms and two triply bridging COs for Pd(4). The two mirror-related doubly bridging COs and the P atom coordinated to Pd(1) approximately conform to a trigonal-planar ligand arrangement consistent with Pd(1) being ideally considered a localized 16-electron system and thereby forming only a weak bonding interaction with Pd(5).

Our later realization and resulting unambiguous evidence that the metal-core composition is Tl_2Pd_{12} instead of Au_2Pd_{12} along with our having carried out $^{31}P\{^1H\}$ COSY NMR measurements not only provided the following interpretation of the NMR pattern but also suggested that **1-Et** maintains a rigid metal-core geometry in solution.

First, the seven most intense resonances in the $^{31}P\{^1H\}$ spectrum of **1-Et** can be modeled in terms of a heteronuclear AA′BXX′ spin-system with *only* ^{31}P–^{31}P couplings within *each* $Pd_3(CO)_3(PEt_3)_3$ unit and ^{31}P–$^{203,205}Tl$ couplings between this unit and the two thallium nuclei ($I = 1/2$ for ^{203}Tl, 29.5%; $I = 1/2$ for ^{205}Tl, 70.5%) on the C_3 axis; hence, this model assumes that the coupling between ^{31}P nuclei of *different* $Pd_3(CO)_3(PEt_3)_3$ units is negligible; the validity of this assumption that the ^{31}P nuclei between the three symmetry-related $Pd_3(CO)_3(PEt_3)_3$ units may be considered uncoupled is predicated on the basis that the ^{31}P nuclei of two adjacent $Pd_3(CO)_3(PEt_3)_3$ units are separated by *five* bonds. The nuclei of B type are ^{31}P nuclei in each of three $Pd_3(CO)_3(PEt_3)_3$ units that lie on the horizontal pseudo-mirror plane of the molecule. The other two mirror-related ^{31}P nuclei within each $Pd_3(CO)_3(PEt_3)_3$ unit belong to the A and A′ type nuclei; the nuclei of X and X′ types are $^{203,205}Tl$ that lie on both sides and cap the central Pd_3 triangle. A $^{31}P\{^1H\}$ NMR simulation spectrum (Fig. 5b)[13] matches well with the observed $^{31}P\{^1H\}$ spectrum of **1-Et** (Fig. 5a). The calculated coupling constants given in Fig. 5b do not distinguish between symmetric and slightly asymmetric $Tl_2Pd_{12}(P)_9$ framework of **1-Et** in solution. In addition, since the observed $^{31}P\{^1H\}$ NMR resonances in the **1-Et** spectrum are broad, no

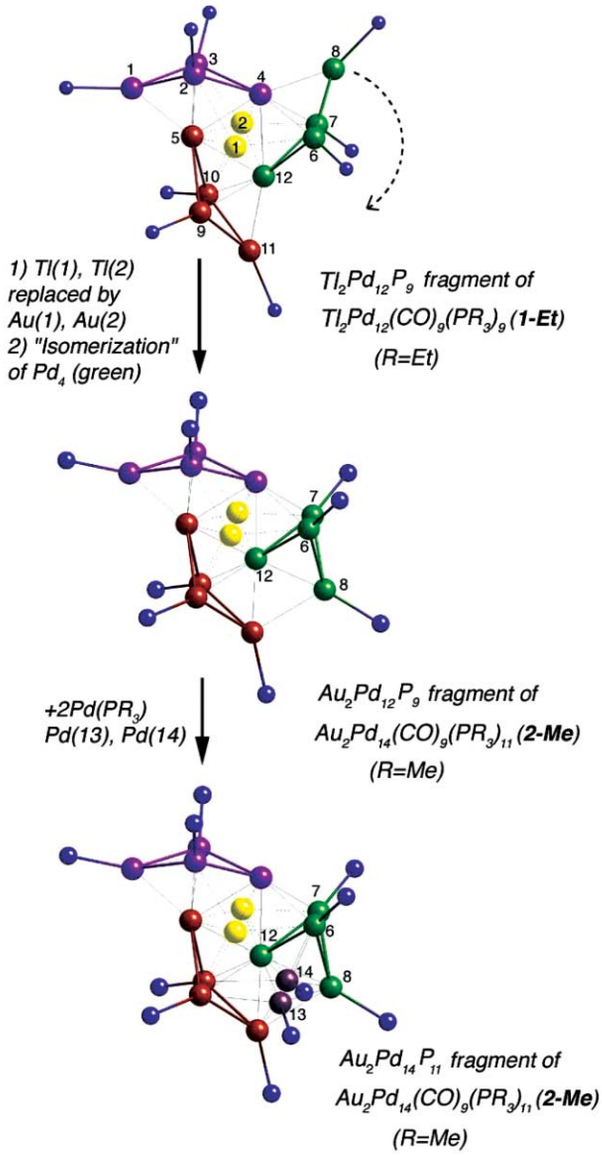

Fig. 4 Stereochemical relationship of entire C_{3h} $M_2Pd_{12}(P)_9$ (M = Tl) fragment in $[Tl_2Pd_{12}(CO)_9(PEt_3)_9]^{2+}$ (**1-Et**), with corresponding isomeric crystallographic C_s (*m*) fragment (M = Au) in $[Au_2Pd_{14}(CO)_9(PR_3)_{11}]^{2+}$ (**2-Me**) (*i.e.*, without Pd(13), Pd(14) and their attached PR_3 ligands). The pseudo-horizontal mirror in **1-Et** corresponds to the crystallographic mirror in **2-Me**. These two $M_2Pd_{12}(P)_9$ fragments in **1-Et** and **2-Me** (M = Tl in **1-Et** and Au in **2-Me**) may be envisioned as two isomeric composites of three Pd_5 trigonal bipyramids joined by edge-sharing to a central M_2Pd_3 trigonal bipyramid. A formal conversion of the palladium framework of **1-Et** into **2-Me** arises from a combined two-step *gedanken* process: (1) bond-cleavage of mirror-containing Pd(8)–Pd(4) connectivity in **1-Et** and formation of mirror-containing Pd(8)–Pd(11) and Pd(8)–Pd(12) bonding connectivities in **2-Me** by the angular pivoting of Pd(8) about the triangular-linked Pd(6)–Pd(7) edge; and (2) addition of two non-adjacent mirror-related capping Pd(13) and Pd(14) atoms with attached PR_3 ligands to two vacant icosahedral sites in **2-Me** to give the observed distorted Pd-centered icosahedral Au_2Pd_{10} cage in **2-Me** that is joined by edge-sharing at Pd(4), Pd(5) with the remaining unperturbed Pd_5 trigonal bipyramid. The similarity of their two preparative routes strongly suggests analogous growth-patterns.

^{31}P–^{31}P coupling was directly observed. The $^3J(^{31}P_A$–$^{31}P_{A'})$ and $^3J(^{31}P_A$–$^{31}P_B)$ coupling constants were estimated to be 3 and 6 Hz, respectively, by use of the WinDNMR software.[13]

Second, to confirm our hypothesis concerning the monomeric nature of **1** in solution, a $^{31}P\{^1H\}$–$^{31}P\{^1H\}$ COSY NMR experiment was conducted on an INOVA-500 Varian NMR instrument. The $^{31}P\{^1H\}$–$^{31}P\{^1H\}$ COSY spectrum is shown in Fig. 6. Letters A–G designate the same resonances in 1D and 2D spectra.

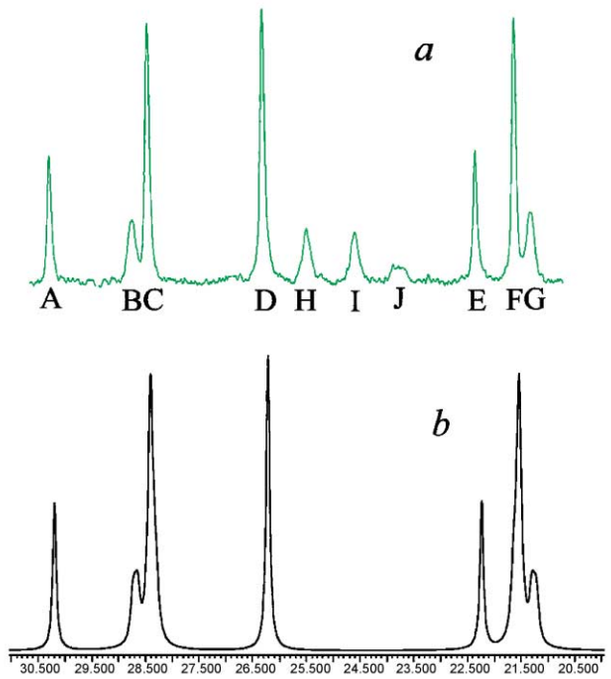

Fig. 5 (a) Observed $^{31}P\{^{1}H\}$ NMR spectra of $[Tl_2Pd_{12}(CO)_9(PEt_3)_9]^{2+}$ dication, **1-Et** ($[PF_6]^-$ salt), in THF-d_8 at room temperature displaying a series of 10 singlets. A corresponding low-temperature spectrum at 190 K exhibited analogous signals. For details see text. (b) Simulated $^{31}P\{^{1}H\}$ NMR spectrum of $[Tl_2Pd_{12}(CO)_9(PEt_3)_9]^{2+}$ assuming AA′BXX′ spin-system with following chemical shifts and coupling constants: $\delta(P_A)$ 24.95, $\delta(P_B)$ 26.2 ppm, $^2J(^{203,205}Tl–^{31}P_A) = -851$, $^3J(^{203,205}Tl–^{31}P_{A'}) = 23$, $^3J(^{203,205}Tl–^{31}P_B) = 484$.

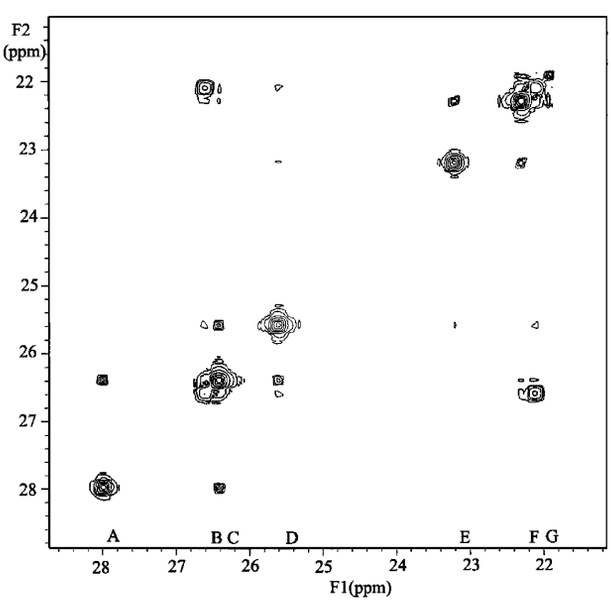

Fig. 6 Observed 2D $^{31}P\{^{1}H\}$ COSY NMR spectrum of **1-Et**. The same peaks in 2D and 1D spectra (Fig. 5) of **1-Et** are denoted with the same letters.

From 2D experiments the following coupling scheme was extracted:

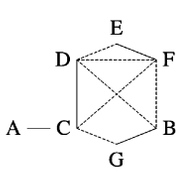

where solid lines represent strong coupling and dashed lines weak coupling. Although not easily explained by an ABB′XX′ spin-system, this coupling scheme still indicates that all seven major signals are coupled in the spectrum; this coupling pattern thereby corresponds to *one* molecular entity, rather than the mixture of several species. The only resonances that are possibly indicative of a dynamic process in solution are those marked as H, I, and J in Fig. 5a (see ref. 12). $^{31}P\{^{1}H\}$ NMR spectra of **1-Et** in THF-d_8, acetone-d_6, DMSO-d_6, and methanol-d_4 showed that the major seven-line spectral pattern did not change, but the resolution and relative intensities of the three small resonances H–J depended on the solvent and concentration. Thus, the $^{31}P\{^{1}H\}$ NMR studies of **1-Et** in different solutions indicate that this cluster is not fluxional in solution.

Geometrical/bonding relationship of $[Tl_2Pd_{12}(CO)_9(PEt_3)_9]^{2+}$ (1-Et) with $[Au_2Pd_{14}(CO)_9(PMe_3)_{11}]^{2+}$ (2-Me)

A geometrical comparison of **1-Et** with the earlier reported **2-Me**[7] reveals a surprising similarity between two structures. The molecular geometry of **2-Me** is shown in Fig. 3. The numbering of the atoms in **2-Me** was changed from the original numbering[7] in order to relate corresponding atoms in **1-Et** and **2-Me**. The metal-core geometry of **2-Me** was described by Mingos *et al.*[7] as a "palladium-centered Au_2Pd_{11} icosahedron which shares an edge with a Pd_5 trigonal bipyramid".

Fig. 4 shows that the entire $M_2Pd_{12}(P)_9$ fragment in **1-Et** (M = Tl) differs from a corresponding $M_2Pd_{12}(P)_9$ fragment in **2-Me** (M = Au) only in the architecture of one $Pd_4(P)_3$ fragment comprised of Pd(6), Pd(7), Pd(8), and Pd(12). This figure also reveals that the Pd_{12} framework in **1-Et** can be formally converted into the Pd_{14} framework in **2-Me** by a two-step *gedanken* transformation: (1) bond-scission of the mirror-containing Pd(4)–Pd(8) connectivity in **1-Et** and formation of mirror-containing Pd(8)–Pd(11) and Pd(8)–Pd(12) bonding connectivities in **2-Me** by the angular pivoting of Pd(8) about the triangular-linked Pd(6)–Pd(7) bonding edge; and (2) addition of two non-adjacent mirror-related capping Pd(13) and Pd(14) atoms with attached PR_3 ligands to two vacant icosahedral sites in **2-Me** to form the observed deformed Pd-centered icosahedral Au_2Pd_{10} cage in **2-Me** that is joined by edge-sharing (at Pd(4) and Pd(5)) with the remaining unperturbed Pd_5 trigonal bipyramid.

Means of corresponding bond lengths and angles in **1-Et** and **2-Me** and one related compound are presented in Table 2. The closeness of these means provides additional support to our interpretation of both structures as being related and formally constructed of three Pd_4 fragments that are emphasized by different colors in Fig. 4. It is somewhat unusual that $5d^{10}$ Au^+ and $6s^2$ $5d^{10}$ Tl^+, being very different chemically, would form two closely related structures with similar corresponding metal–metal bonds. The ability of Pd_4 fragments to act as building blocks in palladium carbonyl phosphine clusters was first proposed in 1990 by Eremenko and Gubin[14a] who visualized the metal-core geometries in Pd_3, Pd_4, Pd_7, Pd_{10}, Pd_{23}, and Pd_{38} carbonyl phosphine clusters as being a combination of triangular Pd_3 and "butterfly" Pd_4 fragments. King[14b] subsequently has illustrated in a review the use of metal triangles as building blocks in metal cluster chemistry.

A salient feature is that both **1-Et** and **2-Me** possess nine bridging COs, of which four of the six doubly bridging COs in **1-Et** are formally transformed into triply bridging COs in **2-Me** due to their dissimilar but yet closely related geometries. Also noteworthy is that the pseudo-horizontal mirror plane in **1-Et** corresponds to the crystallographic mirror plane in **2-Me**.

Comparative cluster electron-counting analysis of $[Tl_2Pd_{12}(CO)_9(PEt_3)_9]^{2+}$ (1-Et) and $[Au_2Pd_{14}(CO)_9(PMe_3)_{11}]^{2+}$ (2-Me) and resulting implications

The observed valence electron count for **1-Et** is 178 (*i.e.*, 2 × 12(Tl) + 12 × 10(Pd) + 9 × 2(CO) + 9 × 2(PEt_3) − 2(+2

Table 2 Comparison of average structural parameters for $[Tl_2Pd_{12}(CO)_9(PEt_3)_9]^{2+}$ (**1-Et**),[f] $[Au_2Pd_{14}(CO)_9(PMe_3)_{11}]^{2+}$(**2-Me**),[g] and $Pd_4(CO)_5(PPh_3)_4$(**4-Ph**)[h]

Connectivity[a]	$[Tl_2Pd_{12}(CO)_9(PEt_3)_9]^{2+}$ [e]	$[Au_2Pd_{14}(CO)_9(PMe_3)_{11}]^{2+}$ [f]	$Pd_4(CO)_5(PPh_3)_4$ [g]
Pd′(c)–Pd′(t)[b]	2.78	2.79	2.75
Pd′(c)–Pd′(c)	2.83	2.86	2.78
Pd′–Pd″(t)[c]	2.80	2.79	—
Pd(i)–M′	2.89	2.94	—
Pd(c)–M′	2.92	2.92	—
M′ ⋯ M′	4.71	4.89	—
Pd–P	2.33	2.34	2.32
Pd–μ_2CO	2.07	2.02	2.11
Pd–μ_3CO	2.07(av.), 2.33	2.13	2.09
μ_2C–O	1.15	1.18	1.15
μ_3C–O	1.16	1.26	1.18
θ/°[d]	145.0	142.2, 67.3	84.5

[a] Palladium designations in **1-Et**, **2-Me**, and **4-Ph** are as follows: Pd(c) – inner basal palladium connected to PR_3 ligand. Pd(t) – outer wingtip palladium connected to PR_3 ligand. Pd(i) – palladium of internal Pd_3 triangle (with no PR_3 ligand). [b] Bonding within Pd_4 fragment. [c] Bonding between adjacent Pd_4 fragments. [d] Dihedral angle of the "butterfly" Pd_4 fragment. [e] M′ = Tl in **1-Et** and Au in **2-Me**. [f] This work. [g] Ref. 7. [h] Ref. 26*a*.

charge) = 178), while that for **2-Me** is 200 (*i.e.*, 2 × 11(Au) + 14 × 10(Pd) + 9 × 2(CO) + 11 × 2(PMe_3) − 2(+2 charge) = 200). Application of the Mingos electron-counting condensation model[15] to **2-Me** (Fig. 3) based upon the condensation of a metal-atom centered icosahedron (170 electrons) with an edge-sharing trigonal bipyramid (72 electrons) would give a valence electron count of 208 electrons (*i.e.*, 170 + 72 − 34 = 208) under the assumption that the normal electron count for a centered icosahedron is 170.[15,16] However, Mingos *et al.*[15b,j] stated in the case of a 13-atom centered icosahedron for which radial bonding interactions predominate (*i.e.*, with tangential surface bonding being negligible) that the electron count is given by $12n_s + \delta_i = (12 \times 12) + 18 = 162$ electrons, where n_s is the number of surface atoms (*viz.*, 12) and δ_i is the electron count characteristic of the central atom or atom-fragment located at the center of the cluster (*viz.*, 18 for one interior Pd atom). The resulting overall valence electron count is then 200 electrons (*i.e.*, 162 + 72 − 34 = 200) which is in exact agreement with the observed electron count. If the edge-sharing Pd_5 trigonal bipyramid and the common Pd_2 edge were likewise formulated as electron-deficient 68 and 30 electron systems, respectively, the calculated count would also be 200 electrons (*i.e.*, 162 + 68 − 30 = 200).

Justification for our use of 162 electrons for the centered icosahedron in **2-Me** is based upon this same number being required for $Pd_{16}(CO)_{13}(PMe_3)_9$, a centered Pd_{13} icosahedron with three exopolyhedral edge-bridging Pd atoms, in order to give a calculated electron count of 204 electrons (*i.e.*, 162 + 3 × 48(triangle) − 3 × 34(edge)) that is identical with the observed value.[16a] Noteworthy is that an identical electron count of 162 electrons is observed in a considerable number of reported centered coinage-metal monoicosahedra containing a central atom M (M = Au, Pd, Pt)[17] including the classic Au-centered Au_{12} cage in $[(\mu_{12}\text{-Au})(AuPMePh_2)_{10}(AuCl)_2]^{3+}$ ($[PF_6]^-$ salt),[17a] the Pd-centered Au_{12} cages in neutral $[(\mu_{12}\text{-Pd})(AuPPh_3)_8(AuCl)_4]$[17b] and $[(\mu_{12}\text{-Pd})(AuPPh_3)_6(Au_2dppe)(AuCl)_4]$,[17c] and the Pt-centered Au_6Ag_6 cage in neutral $[(\mu_{12}\text{-Pt})(AuPPh_3)_6(Ag(\mu_2\text{-I}))_6(\mu_3\text{-Ag})_2]$.[17f]

The necessity in utilizing the lower electron counting value of 162 electrons in order to obtain exact agreement with the observed count for **2** points to the Mingos statement[15b] that this lower value for a centered icosahedron would arise when radial bonding interactions between the centered (interior) metal and 12 surface metal atoms predominate over the tangential ones between the surface metal atoms. For the centered Au_{13} icosahedron in $[(\mu_{12}\text{-Au})(AuPMePh_2)_{10}(AuCl)_2]^{3+}$, Mingos[15b,g] attributed the relatively negligible tangential contributions to the surface-directed valence p_x, p_y AOs per surface gold atom being energetically too high to participate in surface Au–Au bonding; this consequence has been ascribed to relativistic effects being especially large for gold.[18]

Several electron-counting models may be used to describe the *pseudo*-C_{3h} Tl_2Pd_{12} core-geometry of **1-Et** (Fig. 1). If viewed as the condensation of three Pd_5 trigonal bipyramids that share three common edges with a central Tl_2Pd_3 trigonal bipyramid, the overall valence electron count is 186 electrons (*i.e.*, 4 × 72 (trig. bipyr.) − 3 × 34 (edge) = 186). The same valence electron count is also calculated for the core-geometry of **1-Et** being considered either as three Pd_5 trigonal bipyramids connected to a central Pd_3 triangle by edge-sharing together with two capping Tl^+ ions (*i.e.*, 3 × 72 + 48 − 3 × 34 + 2 × 12 = 186) or as three Pd_5 trigonal bipyramids sharing three common vertices along with two capping Tl^+ ions (*i.e.*, 3 × 72 − 3 × 18 + 2 × 12 = 186).

The fact that the calculated electron count for **1-Et** is 8 electrons in excess of its observed count of 178 electrons is not surprising in light of the calculated electron count for **2-Me** also being 8 electrons in excess of its observed count if the normal electron count of 170 electrons is used for the complete centered icosahedron *per se*. However, if **1-Et** were similarly considered as the condensation product of three electron-deficient Pd_5 trigonal bipyramids (68 instead of 72 electrons) that are edge-connected with an electron-deficient Pd_3 triangle (42 instead of 48 electrons) and are capped by two naked Tl^+(12 electrons), the predicted electron count would be 180 electrons (*i.e.*, 3 × 68 + 42 − 3 × 30 + 2 × 12 = 180) which is just 2 electrons in excess of the observed value. This electron-count conformity of both **1-Et** and **2-Me** to electron-deficient models points to the involvement of only the valence 5s AO per surface palladium atom in multicentered metal–metal bonding interactions.[19–21] The reasonably close agreement (Table 2) between corresponding bond-connectivities in **1-Et** and **2-Me** is consistent with this premise. It is noteworthy that the Tl_2Pd_{12} core-geometry in **1-Et** does not conform to a close-packed atomic arrangement but instead is largely composed of face-fused tetrahedra that would be stabilized by multicenter S^σ core-bonding electron-pairs.[19,20]

Stereochemical relationship with other Tl-M clusters (M = Pd, Pt)

That **1-Et** indeed possesses a Tl_2Pd_{12} core (instead of the initially presumed Au_2Pd_{12}) is not without precedence.[22] The existence of analogous neutral $(\mu_3\text{-Tl})Pd_3$ and $(\mu_3\text{-AuPPh}_3)Pd_3$ clusters, obtained from capping of the 44-electron $[Pd_3(\mu_2\text{-}SO_2)_2(\mu_2\text{-Cl})(PPh_3)_4]^-$ monoanion with Tl^+ and $[AuPPh_3]^+$, respectively, had been previously established from mass spectrometry and elemental analysis.[22a] In addition to this only previous example of a Tl–Pd cluster, strong bonding M–Tl–M

interactions (M = Pd, Pt) with relatively short Pd–Tl and Pt–Tl distances of *ca.* 2.8 Å were observed[22b] for analogous zerovalent Pd and Pt metallocryptates with encapsulated Tl(I) atoms. Direct Pd(II)–Tl(I) interactions were also determined[22c] for a heterodinuclear complex containing Pd(II) and Tl(I). In contrast, two kinds of Tl–Pt clusters are known: (1) $[TlPt_3(\mu_2\text{-}CO)_3(PCy_3)_3]^+$, that was quantitatively obtained from the addition of $TlPF_6$ to $Pt_3(\mu_2\text{-}CO)_3(PCy_3)_3$; of importance is that the Tl(I) in its tetrahedral-like $TlPt_3$ core can be readily replaced by $[Au(PCy_3)]^+$ upon reaction with $Au(PCy_3)Cl$;[22d] and (2) a cryptate-like cluster with a sandwich-like Pt_3TlPt_3 core consisting of two $Pt_3(\mu_2\text{-}CO)_3L_3$ moieties held together by three bidentate (LL) $Ph_2P(CH_2)_3PPh_2$ groups (abbreviated as dppp) with an encapsulated Tl(I).[22e] Spectroscopic studies subsequently showed the existence of $[(\mu_3\text{-}Tl)_2Pt_6(\mu_2\text{-}CO)_6(\mu_2\text{-dppm})_3]^{2+}$ with two separate $TlPt_3$ cores.[22f] The fact[22d] that the $TlPt_3$ cluster, $[(\mu_3\text{-}Tl)Pt_3(\mu_2\text{-}CO)_3(PCy_3)_3]^+$, readily converts to the corresponding $(Cy_3P)AuPt_3$ analogue in the presence of $[Au(PCy_3)]^+$ gave rise to our (erroneous) assumption that a Tl–Pd cluster would likewise be transformed into a corresponding Au–Pd cluster in the presence of Au(L)Cl (L = PPh_3, SMe_2).

Synthesis of $[Tl_2Pd_{12}(CO)_9(PEt_3)_9]^{2+}$ (1-Et)

(a) Original synthesis. Because Mingos *et al.*[7] had obtained **2-Me** from the reaction of $Pd_8(CO)_8(PMe_3)_7$[8] with $Au(PCy_3)Cl$ and excess $TlPF_6$ in THF, our initial reactions of $Pd_{10}(CO)_{12}(PEt_3)_6$(**3-Et**) with $Au(PPh_3)Cl$ and excess $TlPF_6$ were also performed in THF. After dissolution of all reagents in THF, the solution rapidly changed color from cherry red to deep brown. Monitoring of the reaction *via* IR spectra in the carbonyl region indicated disappearance of the Pd_{10} precursor within the first 10 min of stirring and subsequent formation of several intermediates. After 25 h of mixing, substantial amounts of dark residue accumulated. To date no crystalline products from these reactions have been isolated.

Our change of solvent from THF to DMF dramatically altered the nature of the reactions. The selection of DMF was based upon the premise that it generally provides a greater stabilization of charged particles and coordinatively unsaturated particles in solution. Under the assumption that the formation of high-nuclearity Au–Pd clusters is a kinetically controlled process, stabilization of intermediates would be extremely important. IR spectra provided definitive evidence that the reactions in DMF proceed through different intermediates. New carbonyl bands at 1873 and 1843 cm^{-1} (subsequently identified as arising from **1-Et**) appeared after mixing of the reactants for 18 h, their intensities maximized after *ca.* 26 h and then gradually decreased. Further stirring of the reaction mixture gave rise to other products that have not been characterized.

Consequently, each reaction was terminated after *ca.* 26 h of stirring with the addition of water in order to precipitate the crude product. The addition of MeOH to the precipitate dissolved a major part of the precipitate. After MeOH removal, the formed residue redissolved almost completely in THF, from which **1-Et** was isolated as the $[PF_6]^-$ salt. The fact that IR and $^{31}P\{^1H\}$ NMR spectra of the extracted crude product before crystallization and corresponding spectra of crystals of **1-Et** are very similar is indicative of the presence of only **1-Et** in the original MeOH extract.

(b) Role of $TlPF_6$. Of course, we had no inkling of the actual importance of $TlPF_6$ other than its presence or absence had a decisive effect on the resulting products. Reactions performed in DMF *without* $TlPF_6$ did not afford **1-Et** but instead led in one reaction to the isolation of the extraordinary nanosized Au–Pd cluster, $Au_5Pd_{45}(CO)_{32}(PEt_3)_{14}$. Details of its synthesis and geometry will be reported elsewhere.

Because $TlPF_6$ has been widely utilized as a chloride scavenger in many reactions involving $Au(PR_3)Cl$, we carried out an NMR investigation which indicated that its function in DMF reactions may be more complex than initially presumed. $^{31}P\{^1H\}$ NMR spectra of $Au(PPh_3)Cl$ in DMF-d_6 were essentially unchanged either in the presence or absence of $TlPF_6$. Upon addition of $TlPF_6$ to $Au(PPh_3)Cl$ in DMF, the solution (which became cloudy due to insoluble TlCl formation) was filtered before NMR measurements were made. In both cases (with and without $TlPF_6$), $^{31}P\{^1H\}$ NMR spectra of $Au(PPh_3)Cl$ expectedly exhibited one signal for the gold-attached PPh_3, but no significant variations in chemical shifts were observed: namely, at 36.70 ppm (without $TlPF_6$) and 36.80 ppm (with $TlPF_6$) along with the characteristic septet resonance centered at −29.50 ppm for the $[PF_6]^-$ anion. This observation of essentially identical $^{31}P\{^1H\}$ chemical shifts with and without $TlPF_6$ in solution indicates that soluble phosphorus-containing fragments that formed upon dissolution of $Au(PPh_3)Cl$ are not affected by the addition of $TlPF_6$.

The $^{31}P\{^1H\}$ NMR results suggest the existence of equilibria between neutral and charged fragments, $Au(PPh_3)Cl \leftrightharpoons [Au(PPh_3)]^+|S_n|Cl^- \leftrightharpoons [Au(PPh_3)]^+ + Cl^-$, that are either shifted toward complete dissociation of $Au(PPh_3)Cl$ into $[Au(PPh_3)]^+$ and Cl^- in DMF solution or at least toward the formation of solvent-separated ion pairs $[Au(PPh_3)]^+|S_n|Cl^-$. This ion-pair formulation presumes that Cl^- ions are sufficiently removed from the $[Au(PPh_3)]^+$ fragment, so that its replacement by $[PF_6]^-$ upon reaction with $TlPF_6$ would not significantly alter the chemical shift at the phosphine. Consequently, we suggest that the presence or absence of Cl^- ions in solution may possibly influence the stabilities of intermediates *formed in the reaction* rather than the initial reagents and that $TlPF_6$ does not simply "activate" $Au(PPh_3)Cl$ by converting it into the $[Au(PPh_3)]^+$ cation (as we initially presumed), because this cation is already present in the reaction medium. Of course, the crucial role of $TlPF_6$ in the reactions is now apparent.

Proposed reaction route to 1-Et and resulting new synthesis with and without $Au(SMe_2)Cl$

In the synthesis of **1-Et** from $Pd_{10}(CO)_{12}(PEt_3)_6$ (**3-Et**) it is important to note that the PEt_3/Pd ratio in the precursor $Pd_{10}(CO)_{12}(PEt_3)_6$ (**3-Et**) is 6/10 (or 0.6), whereas in **1-Et** this ratio is 9/12 (or 0.75). This suggests another growth-process taking place which is parallel to that resulting in the formation of the Tl_2Pd_{12} cluster (**1-Et**). This other process is most likely a slow condensation of the $Pd_{10}(CO)_{12}(PEt_3)_6$ (for example, to $Pd_{23}(CO)_{20}(PEt_3)_{10}$[11b]), because this would lead to the release of free PEt_3, which would then be consumed during formation of the Tl_2Pd_{12} cluster. We do observe a second minor product (which *via* spectral analysis is not the above-mentioned Pd_{23} cluster) that is less soluble in MeOH but dissolves well in THF; as yet crystalline material has not been obtained for X-ray diffraction analysis. The same condensation process would also liberate free CO, which is known to facilitate the formation of $Pd_4(CO)_5(PEt_3)_4$ from $Pd_{10}(CO)_{12}(PEt_3)_6$ in the presence of free phosphine[10a,23]

Our initial (wrong) assumption of the metal-core formulation of **1-Et** as Au_2Pd_{12} suggested a "structure-to-synthesis" approach involving Pd_4 intermediates. It was presumed that in the presence of free CO and PEt_3 the $Pd_{10}(CO)_{12}(PEt_3)_6$ precursor would convert to $Pd_4(CO)_3(PEt_3)_3$ fragments, of which three would condense together with two naked Au^+ to form **1-Et**. In order to substantiate this proposed route, an attempt was made to synthesize **1-Et** by use of the preformed butterfly $Pd_4(CO)_5(PEt_3)_4$ as the palladium precursor instead of $Pd_{10}(CO)_{12}(PEt_3)_6$ (**3-Et**) in the reaction with $Au(PPh_3)Cl$ in the presence of $TlPF_6$. Although this reaction did produce **1-Et**, the yield was much smaller (<5%) than in case of the reaction of **3-Et** with Au(I) and $TlPF_6$. We hypothesized that because $Pd_4(CO)_5(PEt_3)_4$ is fully ligated it may be too stable to react with $Au(PPh_3)Cl$ to give **1-Et**; consequently, in order to "activate"

the $Pd_4(CO)_5(PEt_3)_4$, the gold precursor, $Au(PPh_3)Cl$, was replaced with $Au(SMe_2)Cl$, which is known to act as a phosphine "scavenger" in other reactions. It was presumed that $Au(SMe_2)Cl$ would give rise to partial phosphine elimination from $Pd_4(CO)_5(PEt_3)_4$ and would thereby facilitate the formation of $Pd_4(CO)_3(PEt_3)_3$ fragments that would subsequently condense with Au^+ to form **1-Et**. This approach proved to be highly successful and allowed us to raise the yield of **1-Et** to *ca.* 90%. In light of current knowledge about the true identity of **1-Et**, the seeming necessity of utilizing $Au(SMe_2)Cl$ instead of $Au(PPh_3)Cl$ suggested the following rationalization: namely, that $Au(PPh_3)Cl$ redirects the reaction with **3-Et** and $TlPF_6$ toward other products (thereby producing a low yield of **1-Et**), while $Au(SMe_2)Cl$ indeed acts as a phosphine scavenger (but otherwise does not participate in the reaction in the presence of excess $TlPF_6$) in the formation of the Tl_2Pd_{12} cluster. Subsequently, **1-Et** was obtained in 90% yield from the direct reaction (*i.e.*, without $Au(SMe_2)Cl$) of $Pd_4(CO)_5(PEt_3)_4$ with $TlPF_6$ (mol. ratio, 3/2) in THF.

We have recently prepared $Pd_{10}(CO)_{12}(PMe_3)_6$ (**3-Me**) and are currently attempting to isolate $[Tl_2Pd_{12}(CO)_9(PMe_3)_9]^{2+}$ (**1-Me**).[24] These syntheses and their physical/chemical properties are especially important because palladium carbonyl trimethylphosphine chemistry[15,23] is generally very different from palladium carbonyl triethylphosphine chemistry.[10,24] From direct reaction of $Pd_4(CO)_5(PEt_3)_4$ with $TlPF_6$ we now have isolated an intermediate that provides a much better understanding of the nature of this reaction to form **1-Et**. Details will be given elsewhere.[24,25]

Theoretical analysis

During the course of this research, the following questions arose concerning the existence of $[Tl_2Pd_{12}(CO)_9(PEt_3)_9]^{2+}$ (**1-Et**) (relative to that of the unknown Au_2Pd_{12} analogue) as well as its electronic structure:

(1) Are the interactions between Tl^+, Au^+, and proposed Pd_4 intermediates thermodynamically favorable? (2) Is the unexpected stability of Tl^+ compared to Au^+ for bonding to palladium clusters caused by electronic effects? (3) How do the reactivities of naked and ligated Au(I) compare to the reactivity of Tl^+ in reactions with palladium clusters? (4) How do the atomic charge distributions change in a butterfly Pd_4 framework when it binds Tl^+, Au^+, or $[Au(PPh_3)]^+$, including the extent of delocalization of the positive charge?

Because our computational capabilities did not allow us to investigate the electronic structure of **1-R** with R = H, we chose simpler model systems which hopefully may provide at least qualitative answers to our questions. Because of the lack of exact information about the structures of possible Pd_3- or Pd_4-intermediates, a $Pd_4(CO)_5(PH_3)_4$ model analogous to the geometrically known butterfly $Pd_4(CO)_5(PPh_3)_4$[26] was selected. Results of the geometry-optimization for $Pd_4(CO)_5(PH_3)_4$ in comparison to $Pd_4(CO)_5(PPh_3)_4$ are presented in Table 3. Comparison of geometry optimization results for all four model compounds, $Pd_4(CO)_5(PH_3)_4$, $[TlPd_4(CO)_5(PH_3)_4]^+$, $[AuPd_4(CO)_5(PH_3)_4]^+$, and $[(PH_3)AuPd_4(CO)_5(PH_3)_4]^+$ along with their total energies are presented in Table 4. Natural atomic charges for the four models are presented in Table 5. As in the case of $Au_2Pt_7(CO)_8(PPh_3)_6$ (for which its synthesis, structure, and theoretical analysis will be reported elsewhere),[27] the geometry-optimization of $Pd_4(CO)_5(PH_3)_4$ *via* gradient-corrected DFT calculations gives good agreement of the resulting calculated bond distances (Table 3) with those obtained from the structurally determined $Pd_4(CO)_5(PPh_3)_4$:[26a] the mean error in Pd–Pd bond calculations is 0.6% for the five Pd–Pd bond lengths in $Pd_4(CO)_5(PPh_3)_4$, while the error between the calculated means in $Pd_4(CO)_5(PH_3)_4$ and observed means in $Pd_4(CO)_5(PPh_3)_4$ for the 23 nonhydrogen bonding connectivities is still only 1.7%.[28] A comparative analysis

Table 3 Comparison of experimentally determined molecular parameters of $Pd_4(CO)_5(PPh_3)_4$(**4-Ph**) with corresponding theoretically optimized parameters of $Pd_4(CO)_5(PH_3)_4$

Connectivity[a]	$Pd_4(CO)_5(PPh_3)_4$[b]	$Pd_4(CO)_5(PH_3)_4$	$\|\Delta\|$[c]
Pd(c)–Pd(t)/Å	2.748	2.764	0.016
Pd(c)–Pd(c)/Å	2.775	2.790	0.015
Pd–P/Å	2.320	2.427	0.107
Pd(t)–C(t)/Å	2.171	2.156	0.015
	2.041	2.042	0.001
Pd(c)–C(c)/Å	2.085	2.115	0.030
C(t)–O/Å	1.15	1.194	0.048
C(c)–O/Å	1.18	1.195	0.012
θ/°[d]	84.5	93	8.5

[a] Pd and carbonyl C atoms are designated as follows: Pd(t) – outer wingtip palladium of each butterfly Pd_4 fragment. Pd(c) – inner basal palladium of each butterfly Pd_4 fragment. C(c) – central bridging carbonyl carbon between two Pd(c). C(t) – bridging carbonyl carbon between Pd(c) and Pd(t). [b] Ref. 26*a*. [c] $|\Delta| = |\text{exp} - \text{theor}|$. [d] Dihedral angle between two edge-fused planar $Pd(t)Pd(c)_2$ triangles.

of optimized geometries for the $Pd_4(CO)_5(PH_3)_4$, $[TlPd_4(CO)_5(PH_3)_4]^+$, $[(PH_3)AuPd_4(CO)_5(PH_3)_4]^+$, and $[AuPd_4(CO)_5(PH_3)_4]^+$ models (presented in Table 4) reveal the following trends: upon coordination of the butterfly $Pd_4(CO)_5(PH_3)_4$ with Tl^+, Au^+, or the $[Au(PH_3)]^+$ fragment, the Tl or Au atom occupies an equatorial site of a resulting trigonal-bypiramidal metal-core geometry. All Pd–Pd bonding connectivities lengthened sequentially from $Pd_4(CO)_5(PH_3)_4$, $[TlPd_4(CO)_5(PH_3)_4]^+$, $[(PH_3)AuPd_4(CO)_5(PH_3)_4]^+$ to $[AuPd_4(CO)_5(PH_3)_4]^+$; the mean Pd(c)–Pd(c) and Pd(c)–Pd(t) connectivities (where Pd(c) and Pd(t) denote the inner basal and outer wingtip atoms, respectively) of 2.79 and 2.76 Å in $Pd_4(CO)_5(PH_3)_4$ increase markedly to 3.05 and 2.84 Å, respectively, in $[AuPd_4(CO)_5(PH_3)_4]^+$. A similar trend is observed for the dihedral angle "opening" between the two edge-fused $Pd(c)_2Pd(t)$ triangles in the Pd_4 framework: namely, from 93° in $Pd_4(CO)_5(PH_3)_4$ to virtually identical angles of 147 and 145° in both gold adducts. In contrast, the Pd(c)–M′ and Pd(t)–M′ bonding connectivities (M′ = Au, Tl) decrease sequentially from 3.80 and 2.92 Å in $[TlPd_4(CO)_5(PH_3)_4]^+$ to 2.79 and 2.80 Å, respectively, in $[AuPd_4(CO)_5(PH_3)_4]^+$. These effects are attributed to a significant electron transfer from the palladium framework to the M′ electrophile in the fully symmetric Pd–Pd and Pd–M′ bonding MO of the adduct. A similar bond-length trend was previously shown to occur for *triangulo*-$Pt_3(CO)_3(PR_3)_3$ clusters upon binding to Au^+ or $[Au(PR_3)]^+$ fragments.[9b] The degree of the geometrical distortion in $Pd_4(CO)_5(PH_3)_4$ by the coordinated electrophile may be used as a measure of the electrophile's strength; in the case of Tl^+ coordination to $Pd_4(CO)_5(PH_3)_4$ the optimized geometry of the latter is not distorted nearly as much as in the corresponding geometries with Au^+ or $[Au(PH_3)]^+$ coordination.

Table 5 reveals that upon bonding to $Pd_4(CO)_5(PH_3)_4$, the positive thallium charge decreases from +1 to +0.77, whereas in the $[Au(PH_3)]^+$ and Au^+ adducts there is a much greater decrease in Au charge from +1 to +0.23 and +0.19, respectively; most of this positive charge is redistributed among the CO ligands and phosphorus-attached hydrogen atoms in $Pd_4(CO)_5(PH_3)_4$. This charge redistribution points to a significant electron-density transfer from the CO and PH_3 ligands onto the Au atoms in the Au^+ and $[Au(PH_3)]^+$ adducts as opposed to a much smaller electron-density transfer in the Tl^+ adduct. At the same time, the positive charges on the palladium atoms remain almost unchanged in the two palladium–gold adducts (*viz.*, an average positive charge of +0.22 per Pd in $Pd_4(CO)_5(PH_3)_4$ *versus* that of +0.24 per Pd in $[AuPd_4(CO)_5(PH_3)_4]^+$ and +0.22 per Pd in $[(PH_3)AuPd_4(CO)_5(PH_3)_4]^+$). This signifies that the palladium atoms behave primarily as transducers of the electron density without being

Table 4 Comparison of theoretically optimized molecular parameters of $Pd_4(CO)_5(PH_3)_4$ with corresponding optimized parameters of several Pd_4-based models

Connectivity[a]	$Pd_4(CO)_5(PH_3)_4$	$[TlPd_4(CO)_5(PH_3)_4]^+$	$[(PH_3)AuPd_4(CO)_5(PH_3)_4]^+$	$[AuPd_4(CO)_5(PH_3)_4]^+$
Pd(c)–Pd(t)/Å	2.764	2.781	2.811	2.842
Pd(c)–Pd(c)/Å	2.790	2.835	2.910	3.052
Pd(c)–M′/Å[b]	—	3.802	2.881	2.793
Pd(t)–M′/Å[b]	—	2.921	2.815	2.801
Pd–P/Å	2.427	2.448	2.446	2.427
Pd(t)–C(t)/Å	2.156	2.126	2.172	2.187
	2.042	2.078	2.036	2.027
Pd(c)–C(c)/Å	2.115	2.139	2.187	2.115
C(t)–O/Å	1.194	1.190	1.183	1.188
C(c)–O/Å	1.195	1.185	1.190	1.182
θ/°[c]	93	110	147	145

[a] Pd and carbonyl C atoms are designated as follows: Pd(t) – outer wingtip palladium of each butterfly Pd_4 fragment. Pd(c) – inner basal palladium of each butterfly Pd_4 fragment. C(c) – central bridging carbonyl carbon between two Pd(c). C(t) – bridging carbonyl carbon between Pd(c) and Pd(t). [b] M′ = Au or Tl. [c] Dihedral angle between two planar $Pd(t)Pd(c)_2$ triangles.

Table 5 Calculated total energies and charges for geometrically optimized model systems under C_{2v} symmetry[i]

Species		$Pd_4(CO)_5(PH_3)_4$	$[TlPd_4(CO)_5(PH_3)_4]^+$	$[(PH_3)AuPd_4(CO)_5(PH_3)_4]^+$	$[AuPd_4(CO)_5(PH_3)_4]^+$
	Energy/au	−1106.919467	−1158.418745	−1250.572227	−1242.238043
	Pd	+0.18[a]	+0.08[a]	+0.20[a]	+0.22[a]
		+0.26[b]	+0.27[b]	+0.23[b]	+0.25[b]
Charge per species	CO	−0.29[c]	−0.27[c]	−0.24[c]	−0.21[c]
		−0.32[d]	−0.25[d]	−0.25[d]	−0.24[d]
	P_{Pd}	+0.04[e]	+0.03	+0.04	+0.04
		+0.05[f]	+0.03	+0.04	+0.04
	H	+0.035[g]	+0.06[g]	+0.06[g]	+0.065[g]
	M′[h]	—	+0.77	+0.23	+0.19

[a] Outer wingtip Pd(t) of each butterfly Pd_4 fragment. [b] Inner basal Pd(c) of each butterfly Pd_4 fragment. [c] Bridging CO between Pd(c) and Pd(t). [d] Central bridging CO between two Pd(c). [e] PH_3 ligand attached to outer Pd(t). [f] PH_3 ligand attached to basal Pd(c). [g] Average charge over all P-attached hydrogen atoms. [h] M′ = Au or Tl. [i] Total energy of (a) free PH_3: −8.288300 au, (b) Au^+: −135.141006 au, (c) Tl^+: −51.428337 au, and (d) $[Au(PH_3)]^+$: −143.543378 au and the NPA charge on Au in $[Au(PH_3)]^+$ is +0.60.

directly affected by the charge redistribution. The atomic-charge decrease on each wingtip Pd(t) from +0.18 to +0.08 upon coordination to the Tl^+ in $[TlPd_4(CO)_5(PH_3)_4]^+$ may be caused by a resulting weak back electron transfer from the filled 6s Tl AO to each of the two Pd(t). Although the 6s Tl AO is usually considered to be fully occupied because of the so-called "inert electron pair" effect, some degree of electron transfer from this AO would be expected, especially if it matches well in energy and symmetry with an acceptor orbital. The indicated total electron transfer from the parent $Pd_4(CO)_5(PH_3)_4$ to each electrophilic adduct of $0.23e^-$ in $[TlPd_4(CO)_5(PH_3)_4]^+$, $0.53e^-$ in $[(PH_3)AuPd_4(CO)_5(PH_3)_4]^+$, and $0.81e^-$ in $[AuPd_4(CO)_5(PH_3)_4]^+$ is consistent with Au^+ being the strongest and Tl^+ the weakest electrophile in these models; the observation that $[Au(PH_3)]^+$ is a weaker electrophile than naked Au^+ may be attributed to its PH_3 ligand functioning as an electron donor.

The results of energy calculations for the reactions between Tl^+, Au^+, or $[Au(PH_3)]^+$ with $Pd_4(CO)_5(PH_3)_4$ are presented in the scheme below (with no zero-point energy (ZPE) correction):

$$Pd_4(CO)_5(PH_3)_4 + Tl^+ \longrightarrow [TlPd_4(CO)_5(PH_3)_4]^+ \quad \Delta E_1 = -44 \text{ kcal mol}^{-1}$$

$$Pd_4(CO)_5(PH_3)_4 + [Au(PH_3)]^+ \longrightarrow [(PH_3)AuPd_4(CO)_5(PH_3)_4]^+ \quad \Delta E_2 = -69 \text{ kcal mol}^{-1}$$

$$Pd_4(CO)_5(PH_3)_4 + Au^+ \longrightarrow [AuPd_4(CO)_5(PH_3)_4]^+ \quad \Delta E_3 = -111 \text{ kcal mol}^{-1}$$

$$Au^+ + PH_3 \longrightarrow [Au(PH_3)]^+ \quad \Delta E_{AuP} = -72 \text{ kcal mol}^{-1}$$

The changes in reaction energies ΔE_1 to ΔE_3 follow the same trend as the amount of electron transfer to the electrophile; this electron transfer most likely determines the overall energetics of the reaction. The calculated energy ΔE_{AuP} of the reaction between Au^+ and PH_3 to produce $[Au(PH_3)]^+$ indicates the relative strength of Au–PH_3 bonding in comparison with energies $\Delta E_1 - \Delta E_3$. Although the ΔE_{AuP} is smaller than the ΔE_3 which formally indicates the preference for Au^+ to form an adduct with $Pd_4(CO)_5(PH_3)_4$, the better solvation of the much smaller $[Au(PH_3)]^+$ relative to $[AuPd_4(CO)_5(PH_3)_4]^+$ and the stronger bonding of Au–PR_3 with alkyl R substituents (relative to H ones) would possibly reverse the outcome of the gold bonding preference.

Apparently, the charge delocalization onto the gold atom plays a major role in the stability of the Au–Pd model clusters; in the presence of an additional PH_3 ligand on gold, this stabilization is diminished, which manifests itself in an almost two-fold *decrease* in the total Au–Pd bond energy, such that it becomes comparable with the energy of the Tl–Pd interaction. In turn, the latter can be viewed as primarily an electrostatic rather than covalent interaction, as reflected by the relatively small degree of Tl^+ charge delocalization over the $Pd_4(CO)_5(PH_3)_4$ network and the low bonding energy of the Tl–Pd bonding. The electrostatic nature of the Tl–Pd interaction is probably also responsible for Tl bonding to only the two wingtip Pd(t) (and not both the Pd(t) and Pd(c)); the Pd(t) are presumed to be more nucleophilic than the Pd(c) (*i.e.*, as evidenced by the +0.18 atomic charge on each Pd(t) *versus* +0.26 on each Pd(c) in $Pd_4(CO)_5(PH_3)_4$). Because of the greatly diminished covalent contribution in Tl–Pd bonding, electrons are not transferred onto Tl but instead are localized mainly on each Pd(t), which is in accordance with its lower atomic charge.

Results of the DFT calculations on these four model systems (*viz.*, $Tl^+/[Au(PH_3)]^+/Au^+/Pd_4(CO)_5(PH_3)_4$) have given rise to several qualitative conclusions that may be related to the process of formation of $[Tl_2Pd_{12}(CO)_9(PEt_3)_9]^{2+}$(**1-Et**):

(1) Upon analogous geometrical bonding of Tl^+, $[Au(PH_3)]^+$, or Au^+ to the model butterfly $Pd_4(CO)_5(PH_3)_4$, electron density is transferred mainly from the CO and PH_3 ligands in order to delocalize the positive charge of the electrophile and thereby stabilize the entire system.

(2) Interactions between $Pd_4(CO)_5(PH_3)_4$ and Tl^+, $[Au(PH_3)]^+$, or Au^+ are all thermodynamically favorable processes. However, the strength of an electrophile determines the process energy, the latter being the lowest for Tl^+ adduct and highest for the naked (non-ligated) Au^+ adduct.

(3) The observed preferred formation of the Tl_2Pd_{12} cluster(**1-Et**) instead of either the corresponding unknown Au_2Pd_{12} or $(AuPEt_3)_2Pd_{12}$ ones in the presence of the Au-(SMe_2)Cl reagent may be rationalized on the basis that: (1) any non-ligated Au^+ would rather scavenge a palladium-attached phosphine of a $Pd_4(CO)_5(PEt_3)_4$ precursor than coordinate to palladium fragments; and (2) the electrophilicity of Au-ligated $[Au(PEt_3)]^+$ species is not sufficiently greater than Tl^+ species such that its much greater steric bulk may overcome any electronic effects and thereby prevent an effective condensation with palladium fragments.

Experimental

General comments on materials and techniques

All reactions and manipulations were carried out under an atmosphere of dry nitrogen *via* standard Schlenk techniques. Solvents were dried, saturated with and stored under N_2, and then purged with nitrogen immediately prior to use. The following drying agents were used: THF (K/benzophenone), diisopropyl ether (molecular sieves), acetone ($CuSO_4$), and MeOH (Mg). The DMF solvent was used without additional drying. $AuPPh_3Cl$ and $AuPEt_3Cl$ were purchased from "J&J Materials". All other chemicals were purchased from Strem and used without further purification.

The crystal structure of **1-Et** as the $[PF_6]^-$ salt was determined from X-ray data collected *via* a SMART CCD area detector diffractometry system with a standard Mo sealed-tube generator.[29] All $^{31}P\{^1H\}$ NMR spectra were recorded in either acetone-d_6 or THF-d_8 on a Bruker AM-500 spectrometer (85% H_3PO_4 in D_2O was used as an external reference). Infrared spectra were recorded on a Mattson Polaris FT-IR spectrometer by use of a nitrogen-purged CaF_2 cell. $Pd_{10}(CO)_{12}(PEt_3)_6$ (**3-Et**) was prepared by a modification of the general method of ref. 10*a*.

X-Ray crystallographic analysis of 1-Et

Data are presented for two crystals A and B. Crystal A was selected from a sample that had been obtained from the reaction in DMF of $Pd_{10}(CO)_{12}(PEt_3)_6$ (**3-Et**) with $Au(PPh_3)Cl$ in the presence of $TlPF_6$, while crystal B was chosen from a sample that subsequently had been obtained from the direct reaction of $Pd_4(CO)_5(PEt_3)_4$ and $TlPF_6$ in THF. Dark brown crystals were obtained in both cases by layer or vapor diffusion of hexane into a THF solution. Each crystal was mounted under N_2 on top of a 0.2 mm Lindemann capillary and was fixed with frozen Paratone-N oil at low temperature. The structural determination was obtained from direct methods. Least-squares refinements (on F^2) were carried out with anisotropic displacement parameters for all non-hydrogen atoms. Because both data sets from crystals A and B gave rise to well-determined crystal structures of **1-Et** that were virtually identical (*i.e.*, corresponding mean molecular parameters agreed within 0.02 Å), all X-ray crystallographic results reported herein are arbitrarily based upon the completely ordered crystal A.

$[Tl_2Pd_{12}(CO)_9(PEt_3)_9](PF_6)_2$: $M = 3290.9$ g mol^{-1}, $\lambda = 0.71073$ Å; orthorhombic; *Pbca*; $Z = 8$; $F(000) = 12576$.

Crystal A: $T = 173(2)$ K, $a = 27.366(2)$ Å, $b = 24.416(2)$ Å, $c = 29.905(2)$ Å, $V = 19981(2)$ Å^3, d(calc) = 2.19 Mg m^{-3}. 150,698 reflections obtained over $3.34° \leq 2\theta \leq 52.8°$. Absorption correction (SADABS): μ(Mo-Kα) = 5.27 mm^{-1}; plate-shaped crystal, 0.30 × 0.20 × 0.07 mm^3; max./min. transmission, 0.709/0.301. Anisotropic refinement (911 parameters; zero restraints) on 18,993 independent merged reflections ($R_{int} = 0.068$) converged at $wR_2(F^2) = 0.1388$ for all data; $R_1(F) = 0.0491$ for observed data with $I > 2\sigma(I)$; GOF(on F^2) = 1.149; max./min. residual electron density, 2.07/−0.97 e Å^{-3}.

Crystal B: $T = 100(2)$ K, $a = 27.195(1)$ Å, $b = 24.209(1)$ Å, $c = 29.856(1)$ Å, $V = 19656(1)$ Å^3, d(calc) = 2.22 Mg m^{-3}. 185,791 reflections obtained over $3.12° \leq 2\theta \leq 56.6°$. Absorption correction (SADABS): μ(Mo-Kα) = 5.56 mm^{-1}; block-shaped crystal, 0.43 × 0.27 × 0.23 mm^3; max./min. transmission, 0.357/0.195. Anisotropic refinement (1021 parameters; 16 restraints on disordered Et) on 18,738 independent merged reflections ($R_{int} = 0.114$) converged at $wR_2(F^2) = 0.0953$ for all data; $R_1(F) = 0.0385$ for observed data with $I > 2\sigma(I)$; GOF(on F^2) = 1.080; max./min. residual electron density, 2.39/−1.28 e Å^{-3}.

CCDC reference number 186295.

See http://www.rsc.org/suppdata/dt/b2/b204276m/ for crystallographic data in CIF or other electronic format.

Synthesis of 1-Et from $Pd_{10}(CO)_{12}(PEt_3)_6$ and $Au(PPh_3)Cl$

In a typical reaction, $Au(PPh_3)Cl$ (0.0234 g, 0.047 mmol) dissolved in 5 mL of DMF was added dropwise *via* stainless steel cannula to a stirred solution of $Pd_{10}(CO)_{12}(PEt_3)_6$ (0.100 g, 0.047 mmol) in 10 mL of DMF. After the solution was stirred for 10 min, $TlPF_6$ (0.0455 g, 0.130 mmol) dissolved in 5 mL of DMF was added dropwise to the reaction mixture. The solution changed from a cherry red to a brown color over 30 min. After 26 h the reaction was terminated by slow addition of distilled degassed water to the ice-cooled solution; the resulting dark brown precipitate was filtered and then extracted with three portions of MeOH (5 mL each). After MeOH evaporation, the product was dissolved in THF and crystallized at room temperature from a layering of diisopropyl ether or hexane onto the THF solution. **1-Et** was isolated as dark brown single crystals (estimated yield, 40%).

An IR spectrum of solid **1-Et** in nujol exhibited carbonyl bands at *ca.* 1805 (w, br), 1837 (s) and 1863 (s) cm^{-1}. In THF solution corresponding IR bands occurred at *ca.* 1805 (w, br), 1843 (s) and 1870 (s) cm^{-1}, while in DMF solution bands were observed at *ca.* 1805 (w, br), 1843 (s) and 1869 (s) cm^{-1}.

Synthesis of 1-Et from $Pd_4(CO)_5(PEt_3)_4$ and $TlPF_6$

(a) In the presence of $Au(SMe_2)Cl$, in DMF. In a typical reaction, $Pd_4(CO)_5(PEt_3)_4$ was synthesized *in situ* by the quick addition of 0.04 mL of PEt_3 (0.29 mmol) to the solution of 0.1450 g (0.07 mmol) of $Pd_{10}(CO)_{12}(PEt_3)_6$ (**3-Et**) in 10 mL of DMF under CO atmosphere. After being stirred for 20 min, the CO was replaced by N_2, and $Au(SMe_2)Cl$ (0.0257 g, 0.087 mmol), dissolved in 10 mL of DMF, was quickly added *via* stainless steel cannula to the stirred solution of $Pd_4(CO)_5(PEt_3)_4$. After the solution was stirred for 3–4 min, $TlPF_6$ (0.0683g, 0.195 mmol), dissolved in 5 mL of DMF, was added quickly to the reaction mixture. The solution quickly changed color from cherry red to dark green to brown. After 10–12 h of stirring under N_2, the reaction was terminated by slow addition of distilled degassed water to the ice-cooled solution; the resulting dark brown precipitate was filtered and then extracted with two portions of MeOH (10 mL each). After MeOH evaporation, the product was dissolved in acetone and crystallized from a layering of n-hexane onto the acetone solution. **1-Et** was isolated as dark brown single crystals (estimated yield, 90%).

(b) Without $Au(SMe_2)Cl$, in THF. In a typical reaction, $Pd_4(CO)_5(PEt_3)_4$ was synthesized either *in situ* by the quick addition of 0.04 mL of PEt_3 (0.29 mmol) to a solution of 0.1450 g (0.07 mmol) of $Pd_{10}(CO)_{12}(PEt_3)_6$ (**3-Et**) in 10 mL of THF under CO atmosphere, or as an individual com-

pound.[10a,23] A stoichiometric amount of $TlPF_6$ in THF was then added to a solution of $Pd_4(CO)_5(PEt_3)_4$ under N_2. The reaction color quickly changed first to dark-green and then slowly to brown–red. After 30 min of stirring under N_2, the solvent was evaporated. The solid product was dissolved in acetone and crystallized by vapor diffusion with n-hexane. **1-Et** was isolated as dark-brown single crystals (estimated yield, 90%).

(c) Elemental analysis of 1-Et. An elemental analysis (UW-Madison Soil & Plant Analysis Lab) was obtained *via* ICP-MS analysis on a crystalline sample of **1-Et**. Calculated values are based upon $Tl_2Pd_{12}P_{11}F_{12}O_9C_{63}H_{135}$ (M = 3290.9 g mol^{-1}). Calcd. (found): Au, 0.0 (0.1); Tl, 12.4 (14.6); Pd, 38.8 (36.4); P, 10.4 (10.8) %. The experimental results conclusively show the absence of Au and the presence of Tl as well as Pd and P in reasonable agreement with their calculated values. Noteworthy is that the sample was obtained from the reaction of $Pd_4(CO)_5(PEt_3)_4$ with $TlPF_6$ in the presence of $Au(SMe_2)Cl$.

Theoretical calculations

Quantum chemical calculations were carried out at the gradient-corrected density functional level[30] by use of the hybrid functional B3PW91,[31] which combines the Becke three-fitted parameter functional with a non-local correlation functional from Perdew-Wang-91, implemented in the GAUSSIAN-98 DFT package.[32] Two effective core potentials, LANL2DZ[33] and SDD[34]that are also in GAUSSIAN-98, were used for the metal and phosphorus atoms. These basis sets have quasi-relativistic scalar corrections for Au, Tl, and Pd. Hydrogen, carbon, and oxygen atoms were treated by use of the Dunning/Huzinaga D95 full double-zeta basis set.[35] All structures were optimized to a stationary point, which was checked by IR frequency calculations. Atomic charge distributions, atomic electron configurations, and orbital energies were calculated with the NBO program[36] that is included in the Gaussian-98 package.

Acknowledgements

This research was supported by the National Science Foundation (Grant CHE-9729555). Departmental purchase of a CCD area detector system was made possible by funds from NSF (Grant CHE-9310428), the UW-Madison Graduate School, and the Chemistry Department. Departmental purchase of the Varian UNITY-500 NMR was partially made possible by funds from NSF CHE-9629688 and of the Bruker AC-300 NMR by funds from NSF CHE-9208963 and NIH 1 S10 RRO8389–01. We gratefully thank Professors Clark Landis and Frank Weinhold for theoretical discussions, Professor Hans Reich for NMR discussions, Dr. Charles Fry for experimental NMR assistance, and Dr. Ilia Guzei for crystallographic advice. We also epxress our sincere appreciation to one referee for his effort (footnote 12) to interpret the $^{31}P\{^1H\}$ NMR solution spectrum of the then presumed Au_2Pd_{12} cluster (**1-Et**). Computational resources provided to the UW Chemistry Parallel Computing Center through NSF Grant CHE0091916 and gifts from the Intel Corporation are gratefully acknowledged. Color figures were prepared with Crystal Maker, Interactive Crystallography (version 5). David C. Palmer (P.O. Box 183 Bicester, Oxfordshire, UK OXG 7BS).

References and notes

1 (*a*) J.-L. Malleron, J.-C. Fiaud and J. Y. Legros, *Handbook of Palladium Catalyzed Organic Reactions*, Academic Press, San Diego, CA, 1997; (*b*) J.-L. Malleron, A. Juin, *Database of Palladium Chemistry*, Academic Press, San Diego, CA, 1997; (*c*) W. M. H. Sachtler and A. Yu. Stakheev, *Catal. Today*, 1992, **12**, 283 and references therein; (*d*) Z. Zhang, A. P. Cavalcanti and W. M. H. Sachtler, *Catal. Lett.*, 1992, **12**, 157; (*e*) Z. Zhang, L. Xu and W. M. H. Sachtler, *J. Catal.*, 1991, **131**, 502; (*f*) L. Xu, G.-D. Lei, W. M. H. Sachtler, R. D. Cortright and J. A. Dumesic, *J. Phys. Chem.*, 1993, **97**, 11517 and references therein; (*g*) J. H. Sinfelt, *Bimetallic Catalysts: Discoveries, Concepts, and Applications*, J. Wiley & Sons, New York, 1983, pp. 1–164; and references therein; (*h*) J. H. Sinfelt, *Acc. Chem. Res.*, 1987, **20**, 134; (*i*) P. Gallezot, *"Metal Clusters in Zeolites," in Metal Clusters*, ed. M. Moskovits, J. Wiley, New York, 1986, pp. 219–247; (*j*) B. C. Gates, *Catalytic Chemistry*, J. Wiley, New York, 1992; (*k*) P. R. Raithby, *Platinum Met. Rev.*, 1998, **42**, 146 and references therein; (*l*) V. Ponec, *Adv. Catal.*, 1983, **32**, 149; (*m*) P. Braunstein and J. Rose, in *Comprehensive Organometallic Chemistry II*, ed. E. W. Abel, F. G. A. Stone and G. Wilkinson, Elsevier, Tarrytown, NY, 1995, vol. 10, ed. R. D. Adams, ch. 7, 351; (*n*) G. Süss-Fink and G. Meister, *Adv. Organomet. Chem.*, 1993, **35**, 41; (*o*) *Catalysis by Di- and Polynuclear Metal Cluster Complexes*, ed. R. D. Adams and F. A. Cotton, Wiley-VCH, New York, 1998; (*p*) *Metal Clusters in Chemistry*, ed. P. Braunstein, L. A. Oro and P. R. Raithby, Wiley-VCH, New York, 1999, vol. 2; (*q*) *Handbook of Heterogeneous Catalysis*, ed. G. Ertl, H. Knözinger and J. Weitkamp, Wiley-VCH, New York, 1994; (*r*) *Applied Homogeneous Catalysis with Organometallic Compounds*, ed. B. Cornils and W. A. Herrmann, Wiley-VCH, New York; vol. 1 (Applications), 1996; *Applied Homogeneous Catalysis with Organometallic Compounds*, ed. B. Cornils and W. A. Herrmann, Wiley-VCH, New York, vol. 2 (Developments), 1996; (*s*) I. D. Salter, *Adv. Organomet. Chem.*, 1989, **29**, 249; (*t*) I. D. Satler, in *Comprehensive Organometallic Chemistry II*, ed. E. W. Abel, F. G. A. Stone and G. Wilkinson, Elsevier, Tarrytown, NY, 1995, vol. 10, ed. R. D. Adams, ch. 5, p. 255; (*u*) I. D. Salter, in *Metal Clusters in Chemistry*, ed. P. Braunstein, L. A. Oro and P. R. Raithby, Wiley-VCH, New York, 1999, vol. 1, p. 509; (*v*) S.-M. Lee and W.-T. Wong, *J. Cluster Sci.*, 1998, **9**, 417; (*w*) I. I. Moiseev and M. N. Vargaftik, *New J. Chem.*, 1998, **22**, 1217; (*x*) T. A. Stromnova and I. I. Moiseev, *Russ. Chem. Rev.*, 1998, **67**, 485.

2 (*a*) L. H. Pignolet, M. A. Aubart, K. L. Craighead, R. A. T. Gould, D. A. Krogstad and J. S. Wiley, *Coord. Chem. Rev.*, 1995, **143**, 219 and references therein; (*b*) D. A. Krogstad, W. V. Konze and L. H. Pignolet, *Inorg. Chem.*, 1996, **35**, 6763 and references therein; (*c*) M. A. Aubart and L. H. Pignolet, *J. Am. Chem. Soc.*, 1992, **114**, 7901; (*d*) T. G. M. M. Kappen, J. J. Bour, P. P. J. Schlebos, A. M. Roelofsen, J. G. M. van der Linden, J. J. Steggerda, M. A. Aubart, D. A. Krogstad, M. F. J. Schoondergang and L. H. Pignolet, *Inorg. Chem.*, 1993, **32**, 1074; (*e*) M. A. Aubart, B. D. Chandler, R. A. T. Gould, D. A. Krogstad, M. F. T. Schoondergang and L. H. Pignolet, *Inorg. Chem.*, 1994, **33**, 3724; (*f*) M. A. Aubart, J. F. D. Koch and L. H. Pignolet, *Inorg. Chem.*, 1994, **33**, 3852; (*g*) L. I. Rubenstein and L. H. Pignolet, *Inorg. Chem.*, 1996, **35**, 6755; (*h*) I. V. G. Graf, J. W. Bacon, M. B. Consugar, M. E. Curley, L. N. Ito and L. H. Pignolet, *Inorg. Chem.*, 1996, **35**, 689.

3 (*a*) M. Ichikawa, *Advances in Catalysis*, 1992, **38**, 283 and references therein; (*b*) L. Markó and A. Vizi Orosz, *"Homogeneous Catalysis By Metal Clusters," in Metal Clusters in Catalysis*, ed. B. C. Gates and H. Knözinger, Elsevier, New York, 1986, pp. 89–120; (*c*) L. Guczi, *"Supported Bimetallic Catalysts Derived from Molecular Metal Clusters," in Metal Clusters in Catalysis*, ed. B. C. Gates and H. Knözinger, Elsevier, New York, 1986, pp. 547–609; (*d*) M. Ichikawa, *Platinum Met. Rev.*, 2000, **44**, 3 and references therein.

4 T. Kimura, A. Fukuoka, A. Fumagalli and M. Ichikawa, *Catal. Lett.*, 1989, **2**, 227.

5 (*a*) H. Bönnemann and R. M. Richards, *Eur. J. Inorg. Chem.*, 2001, 2455; (*b*) N. Toshima and T. Yonezawa, *New J. Chem.*, 1998, **22**, 1179.

6 N. T. Tran, D. R. Powell and L. F. Dahl, *Angew. Chem., Int. Ed.*, 2000, **39**, 4121.

7 R. Copley, C. M. Hill and D. M. P. Mingos, *J. Cluster Sci.*, 1995, **6**(1), 71.

8 M. Bochmann, I. Hawkins, M. B. Hursthouse and R. L. Short, *Polyhedron*, 1987, **6**, 1987.

9 (*a*) A. D. Burrows and D. M. P. Mingos, *Transition Met. Chem.*, 1993, **18**, 129; (*b*) A. D. Burrows and D. M. P. Mingos, *Coord. Chem. Rev.*, 1996, **154**, 19.

10 (*a*) E. G. Mednikov, N. K. Eremenko, S. P. Gubin, Yu. L. Slovokhotov and Yu. T. Struchkov, *J. Organomet. Chem.*, 1982, **239**, 401; E. G. Mednikov and N. K. Eremenko, *Russ. Chem. Bull.*, 1983, **32**, 2240 (Engl. Transl.); (*b*) D. M. P. Mingos and C. M. Hill, *Croat. Chim. Acta*, 1995, **68**(4), 745.

11 (*a*) E. G. Mednikov, Yu. L. Slovokhotov and Yu. T. Struchkov, *Metalloorg. Khim.*, 1991, **4**, 123 (*Organomet. Chem. USSR*, 1991, **4**, 65 (Engl. Transl.)); (*b*) E. G. Mednikov, N. K. Eremenko, Yu. L. Slovokhotov and Yu. T. Struchkov, *J. Organomet. Chem.*, 1986, **301**,

C35; E. G. Mednikov, *Organomet. Chem. USSR*, 1991, **4**, 433 (Engl. Transl.); (*c*) E. G. Mednikov, N. K. Eremenko, Yu. L. Slovokhotov and Yu. T. Struchkov, *Zh. Vses. Khim. O-va. im. D. I. Mendeleeva*, 1987, **32**, 101 (Russ.); E. G. Mednikov, *Russ. Chem. Bull.*, 1993, **42**, 1242; (*d*) E. G. Mednikov and N. I. Kanteeva, *Russ. Chem. Bull.*, 1995, **44**, 163; (*e*) E. G. Mednikov, N. K. Eremenko, Yu. L. Slovokhotov and Yu. T. Struchkov, *J. Chem. Soc., Chem. Commun.*, 1987, 218.

12 Based upon the stoichiometry of **1-Et** conforming to the misassigned Au_2Pd_{12} core, one referee proposed that the $^{31}P\{^1H\}$ NMR spectrum could be interpreted as an overlapping AB_2 pattern that is in complete accordance with its solid-state geometry. The following interpretation was given: "The A component is a standard 1 : 2 : 1 triplet centered at 26.2 ppm (side peaks at 30.2 and 22.3 ppm). The B2 component is a non-first order pattern centered at 25.0 ppm and is roughly a doublet (28.4 and 21.5 ppm) but with additional small components to each side of the two main peaks. The small peak at 23.8 ppm is evidently an impurity. The interpretation shows these two patterns to be in a 3 : 6 ratio as expected for the cluster which has three sets of 2 : 1 phosphine ligands on adjacent Pd centers". Although not in agreement with the above explanation (see below), we greatly appreciate the referee's time and effort to provide an appropriate description. Our rejection of the referee's seemingly apparent interpretation of the observed $^{31}P\{^1H\}$ NMR spectrum of **1-Et** (also contingent on our initial mistaken formulation as $[Au_2Pd_{12}(CO)_9(PEt_3)_9]^{2+}$) as an overlapping AB_2 coupling pattern that exactly matches the crystalline-state structure is based upon the following reasons: (1) Firstly, A and B components of an AB_2-type $^{31}P\{^1H\}$ NMR spectrum can never overlap without losing their fine structure. Under the assumption that A-type nuclei are more deshielded than B-type nuclei in a molecule, the most downfield resonance from an A-type nuclei group is *always* more upfield than the most up-field resonance from a B-type nuclei group. In the limiting case when the chemical shifts of A- and B-type nuclei coincide, the resonances of both the A- and B-type groups degenerate into one singlet. (2) Secondly, most ^3J(P–P) coupling constants in palladium phosphine carbonyl clusters are not greater than 60 Hz; in sharp contrast, an estimation of ^3J(P–P) from an assumed triplet signal (centered at 26.2 ppm with side peaks at 30.2 and 22.3 ppm) gives rise to an unusually large value of 485 Hz. (3) Thirdly, weak resonances between 23 and 26 ppm cannot be readily dismissed as impurities in that they have been reproduced in all solution spectra of both crystalline and powder material of **1-Et** obtained from different reactions (*viz.*, from reactions of $Pd_{10}(CO)_{12}(PEt_3)_6$ with $Au(PPh_3)Cl$ and $TlPF_6$, and of $Pd_4(CO)_5(PEt_3)_4$ with $Au(SMe_2)Cl$ and $TlPF_6$). Depending upon sample preparation, $^{31}P\{^1H\}$ NMR spectra revealed these small resonances to be either fully resolved or coalesced into one broad resonance. Spectral resolution was usually achieved by slight solvent dilution of the sample, which may be indicative of molecular dynamic processes in solution.

13 WinDNMR, Dynamic NMR Spectra for Windows, H. J. Reich, *J. Chem. Educ.: Software*, 1996, 3C2; H. J. Reich, *J. Chem. Educ.: Software*, 2001, SP28.

14 (*a*) N. K. Eremenko and S. P. Gubin, *Pure Appl. Chem.*, 1990, **62**, 1179; (*b*) R. B. King, *J. Cluster Sci.*, 1995, **6**, 5.

15 (*a*) D. M. P. Mingos, *J. Chem. Soc., Chem. Commun.*, 1983, 706; (*b*) D. M. P. Mingos, *J. Chem. Soc., Chem. Commun.*, 1985, 1352; (*c*) D. M. P. Mingos, *Acc. Chem. Res.*, 1984, **17**, 311; (*d*) D. M. P. Mingos, *Polyhedron*, 1984, **3**, 1289; (*e*) K. P. Hall and D. M. P. Mingos, *Prog. Inorg. Chem.*, 1984, **32**, 237; (*f*) D. M. P. Mingos and R. L. Johnson, *J. Organomet. Chem.*, 1985, **280**, 419; (*g*) D. M. P. Mingos and L. Zhenyang, *J. Chem. Soc., Dalton Trans.*, 1988, 1657 and references therein; (*h*) D. M. P. Mingos and A. P. May, in *The Chemistry of Metal Cluster Complexes*, ed. D. F. Shriver, H. D. Kaesz and R. D. Adams, VCH Publishers, New York, 1990, ch. 2, pp. 11–119; (*i*) D. M. P. Mingos and D. J. Wales, *Introduction to Cluster Chemistry*, Prentice Hall, Old Tappan, NJ, 1990; (*j*) D. M. P. Mingos and M. J. Watson, *Adv. Inorg. Chem.*, 1992, **39**, 327.

16 (*a*) N. T. Tran, M. Kawano and L. F. Dahl, *J. Chem. Soc., Dalton Trans.*, 2001, 2731; (*b*) see footnote 32 in ref. 17(*a*).

17 (*a*) C. E. Briant, B. R. C. Theobald, J. W. White, L. K. Bell, D. M. P. Mingos and A. J. Welch, *J. Chem. Soc., Chem. Commun.*, 1981, **201**; (*b*) M. Lapp and J. Strähle, *Angew. Chem., Int. Ed. Engl.*, 1994, **33**, 207; (*c*) R. C. B. Copley and D. M. P. Mingos, *J. Chem. Soc., Dalton Trans.*, 1992, 1755; (*d*) B. K. Teo, H. Dang, H. Zhang, as quoted in H. Zhang and B. K. Teo, *Inorg. Chim. Acta*, 1997, **265**, 213; (*e*) B. K. Teo and H. Zhang, *J. Organomet. Chem.*, 2000, **614**, 66.

18 (*a*) N. Rösch, A. Görling, D. E. Ellis and H. Schmidbaur, *Angew. Chem., Int. Ed. Engl.*, 1989, **28**, 1357; (*b*) P. Pyykkö, *Chem. Rev.*, 1988, **88**, 593; (*c*) V. Bonacic-Koutecky, P. Fantucci and J. Koutecky, *Chem. Rev.*, 1991, **91**, 1035; (*d*) K. S. Pitzer, *Acc. Chem. Res.*, 1979, **12**, 271; (*e*) K. Balasubramanian, *J. Phys. Chem.*, 1989, **93**, 6585; (*f*) P. Schwerdtfeger and P. D. W. Boyd, *Inorg. Chem.*, 1992, **31**, 327; (*g*) P. Pyykkö and Y. Zhao, *Angew. Chem., Int. Ed. Engl.*, 1991, **30**, 604.

19 A similar qualitative bonding description[20b] of the T_d $[Au_6Ni_{12}(CO)_{24}]^{2-}$ cluster[20] involving delocalized interoctahedral S^σ core-bonding electron pairs was used to reconcile the calculated results[20b] from the Fenske–Hall MO method (ref. 21).

20 (*a*) A. J. Whoolery and L. F. Dahl, *J. Am. Chem. Soc.*, 1991, **113**, 6683; (*b*) A. J. Woolery Johnson, B. Spencer and L. F. Dahl, *Inorg. Chim. Acta*, 1994, **227**, 269.

21 M. B. Hall and R. F. Fenske, *Inorg. Chem.*, 1972, **11**, 768.

22 (*a*) A. D. Burrows, J. C. Machell and D. M. P. Mingos, *J. Chem. Soc., Dalton Trans.*, 1992, 1939; (*b*) V. J. Catalano, B. L. Bennett, R. L. Yson and B. C. Noll, *J. Am. Chem. Soc.*, 2000, **122**, 10056; (*c*) A. L. Balch, B. J. Davis, E. Y. Fung and M. M. Olmstead, *Inorg. Chim. Acta*, 1993, **212**, 149; (*d*) O. J. Ezomo, D. M. P. Mingos and I. D. Williams, *J. Chem. Soc., Chem. Commun.*, 1987, 924; (*e*) L. Hao, J. J. Vittal and R. J. Puddephatt, *Organometallics*, 1996, **15**, 3115; L. Hao, J. J. Vittal and R. J. Puddephatt, *Inorg. Chem.*, 1996, **35**, 269; (*f*) G. J. Spivak, J. J. Vittal and R. J. Puddephatt, *Inorg. Chem.*, 1998, **37**, 5474.

23 E. G. Mednikov and N. K. Eremenko, *Izv. Akad. Nauk SSSR, Ser. Khim.*, 1982, 2540 (*Russ. Chem. Bull.*, 1982, **31**, 2240 (Engl. Transl.)).

24 S. A. Ivanov, E. G. Mednikov, R. V. Nichiporuk, and L. F. Dahl, unpublished research, 2002.

25 E. G. Mednikov, S. A. Ivanov, and L. F. Dahl, unpublished research, 2002.

26 (*a*) R. D. Feltham, G. Elbaze, R. Ortega, C. Eck and J. Dubrawski, *Inorg. Chem.*, 1985, **24**, 1503; (*b*) E. G. Mednikov, N. K. Eremenko, Yu. L. Slovokhotov, Yu. T. Struchkov and S. P. Gubin, *Sov. J. Coord. Chem.*, 1987, **13**(7), 979; (*c*) N. K. Eremenko, E. G. Mednikov and S. P. Gubin, *Sov. J. Coord. Chem.*, 1984, **10**, 340.

27 S. A. Ivanov, M. A. Kozee, N. de Silva and L. F. Dahl, to be published.

28 $$\text{Mean error} = \sum_{i=1}^{N_b} \frac{|\, d_{exp} - d_{theor} \,|}{N_b d_{exp}} \times 100\%$$

where d_{exp} denotes the crystallographically determined bond length, d_{theor} denotes calculated bond length, and N_b denotes the number of bonds used to calculate the error.

29 G. Sheldrick, *SHELXTL (version 5.1)*, program library, Bruker Analytical X-Ray Systems, Madison, WI.

30 W. Kohn and L. J. Sham, *Phys. Rev.*, 1965, **140**, A1133.

31 (*a*) A. D. Becke, *J. Chem. Phys.*, 1993, **98**, 5648; (*b*) K. Burke, J. P. Perdew, Y. Wang, in *Electronic Density Functional Theory: Recent Progress and New Directions*, ed. J. F. Dobson, G. Vignale and M. P. Das, Kluwer Academic/Plenum, New York, 1998; (*c*) J. P. Perdew, J. A. Chevary, S. H. Vosko, K. A. Jackson, M. R. Pederson, D. J. Singh and C. Fiolhais, *Phys. Rev. B*, 1992, **46**, 6671; J. P. Perdew, J. A. Chevary, S. H. Vosko, K. A. Jackson, M. R. Pederson, D. J. Singh and C. Fiolhais, *Phys. Rev. B*, 1993, **48**, 4978; (*d*) J. P. Perdew, K. Burke and Y. Wang, *Phys. Rev. B*, 1996, **54**, 165333.

32 M. J. Frisch, G. W. Trucks, H. B. Schlegel, G. E. Scuseria, M. A. Robb, J. R. Cheeseman, V. G. Zakrzewski, J. A. Montgomery, Jr., R. E. Stratmann, J. C. Burant, S. Dapprich, J. M. Millam, A. D. Daniels, K. N. Kudin, M. C. Strain, O. Farkas, J. Tomasi, V. Barone, M. Cossi, R. Cammi, B. Mennucci, C. Pomelli, C. Adamo, S. Clifford, J. Ochterski, G. A. Petersson, P. Y. Ayala, Q. Cui, K. Morokuma, D. K. Malick, A. D. Rabuck, K. Raghavachari, J. B. Foresman, J. Cioslowski, J. V. Ortiz, A. G. Baboul, B. B. Stefanov, G. Liu, A. Liashenko, P. Piskorz, I. Komaromi, R. Gomperts, R. L. Martin, D. J. Fox, T. Keith, M. A. Al-Laham, C. Y. Peng, A. Nanayakkara, C. Gonzalez, M. Challacombe, P. M. W. Gill, B. G. Johnson, W. Chen, M. W. Wong, J. L. Andres, M. Head-Gordon, E. S. Replogle and J. A. Pople, *Gaussian 98 (Revision A.6)*, Gaussian, Inc., Pittsburgh, PA, 1998.

33 (*a*) P. J. Hay and W. R. Wadt, *J. Chem. Phys.*, 1985, **82**, 270–299; (*b*) W. R. Wadt and P. J. Hay, *J. Chem. Phys.*, 1985, **82**, 284.

34 Ref. 225–248 in the manual for Gaussian 98 (ref. 32).

35 T. H. Dunning, Jr. and P. J. Hay, in *Modern Theoretical Chemistry*, ed. H. F. Schaefer, III, Plenum, New York, 1976, vol. 3, p. 1.

36 (*a*) E. D. Glendening, J. K. Badenhoop, A. E. Reed, J. E. Carpenter and F. Weinhold, *NBO 4.0*, Theoretical Chemistry Institute, University of Wisconsin, Madison,1994; (*b*) A. E. Reed, L. A. Curtiss and F. Weinhold, *Chem. Rev.*, 1988, **88**, 899; (*c*) F. Weinhold, *Natural bond orbital methods*, in *Encyclopedia of Computational Chemistry*, ed. P. v. R. Schleyer, N. L. Allinger, T. Clark, J. Jasteiger and P. A. Kollman, Wiley, Chichester, UK, 1998, vol. 3, pp. 1792–1811; (*d*) F. Weinhold and C. R. Landis, *Chem. Educ.: Res. Pract. Eur.*, 2001, **2**, 91.